

Article

# Sensitivity Simulations of Wind-driven Water Circulation in İzmit Bay

Sabri Mutlu <sup>1,2,\*</sup>, Barış Önel <sup>1</sup>, Mehmet Ilıcak <sup>3</sup> and Hüsne Altıok <sup>4</sup>

<sup>1</sup> Aeronautics and Astronautics Faculty, Meteorological Engineering, Istanbul Technical University, Istanbul 34469, Türkiye; onolba@itu.edu.tr

<sup>2</sup> Climate Change and Sustainability VP, TÜBİTAK Marmara Research Center, Kocaeli 41470, Türkiye

<sup>3</sup> Eurasia Institute of Earth Sciences, Istanbul Technical University, Istanbul 34469, Türkiye; milicak@itu.edu.tr

<sup>4</sup> Institute of Marine Sciences and Management, Istanbul University, Istanbul 34134, Türkiye; altiokh@istanbul.edu.tr

\* Correspondence: mutlu16@itu.edu.tr or sabri.mutlu@tubitak.gov.tr; Tel.: +90-262-6772990

**Abstract:** İzmit Bay, a 50 km long inlet at the eastern end of the Marmara Sea, is crucial for the region's economy, culture, and marine ecosystem. The bay's water circulation regulates nutrient distribution, stratification, sedimentation, oxygen levels, heat, and pollution levels. It is also influenced by meteorological events, such as short-term moderate to strong wind conditions. This study investigated the sensitivity of İzmit Bay Water Circulation to wind speed, direction, and duration using the MITgcm model with Orlanski boundary conditions and process-oriented modeling. The simulations showed that under weak forcing conditions, seawater temperature, salinity, and stratification do not significantly vary. However, strong forcing and wind speeds (statistically defined by percentiles of observation data) of 4.9 m/s (75%), 6.7 m/s (90%), and 10.1 m/s (99%) generate significant mesoscale and sub-mesoscale processes, depending on the direction. Westerly component winds cause downwelling at the eastern coastline, while easterly component winds bring sub-surface water to the surface. Strong winds from N, NE, and E sectors lead to the rise in lower-layer waters in the western basin, forcing them to overflow through the Hersek Delta sill into the central basin. Overall, severe wind events greater than 4.9 m/s (75%) significantly affect the bay's hydrography by transforming the upper layer, with a decrease in temperature up to 5 °C and an increase in salinity up to 10 ppt.

**Keywords:** İzmit Bay; wind forcing; sensitivity simulations; MITgcm; upwelling



**Citation:** Mutlu, S.; Önel, B.; Ilıcak, M.; Altıok, H. Sensitivity Simulations of Wind-driven Water Circulation in İzmit Bay. *J. Mar. Sci. Eng.* **2024**, *12*, 824. <https://doi.org/10.3390/jmse12050824>

Academic Editor: João Miguel Dias

Received: 29 March 2024

Revised: 3 May 2024

Accepted: 8 May 2024

Published: 15 May 2024



**Copyright:** © 2024 by the authors. Licensee MDPI, Basel, Switzerland. This article is an open access article distributed under the terms and conditions of the Creative Commons Attribution (CC BY) license (<https://creativecommons.org/licenses/by/4.0/>).

## 1. Introduction

The Marmara Sea is a relatively small, landlocked sea (~11,500 km<sup>2</sup>); it has many distinctive physical properties [1–6]. In a layered structure, there are primarily two different water masses. Less saline but very productive Black Sea-origin water (~18 ppt) is floating over anoxic (~38.5 ppt) Mediterranean Sea-origin water. Due to mixing in the İstanbul Strait and seasonal weather conditions, the temperature and salinity of the upper-layer water varies between approximately 8.0 °C and 28.4 ppt in winter and 25 °C and 23.5 ppt in summer. Conversely, there is a slight seasonal change in the lower layer (~15.2 °C and ~38.5 ppt). At 25 m depth, a salinity-driven sharp pycnocline with low levels of mixing exists between these layers. This pycnocline is generally accepted as permanent since even the abrupt cooling of surface waters in winter is not able to break this structure [6]. On the other hand, severe weather events involving strong winds can erode the pycnocline down to deeper levels, down to about 40 m [2]. The basin-wide mixing and circulation seen on the surface is under two main drivers: weather events and the İstanbul Strait Jet. The jet reaches the southern coast and isolates İzmit Bay from the rest of the circulation of the Marmara Sea, thereby limiting its flushing effect and adversely affecting the environmental

status of the bay [7]. The jet also bends and converges with the gyre in the center of the basin. Eventually, it splits into many branches and leaves the basin via the Çanakkale Strait.

Chiggiato et al. [8] used the Regional Ocean Modelling System (ROMS) to simulate general circulation in the Marmara Sea realistically. They also investigated the role of various dynamics in determining the Marmara Sea's circulation and pycnocline structure using additional idealized numerical experiments. They observed large displacements of the pycnocline depth during the sea trials. These were interpreted as storm-driven upwelling/downwelling dynamics associated with northeasterly winds [8]. Sannino et al. [9] preferred using the Massachusetts Institute of Technology general circulation model (MIT-gcm) to simulate the sea, presenting full details of its unique and contrasting properties. The intense surface jet emerging from the İstanbul Strait was found to control the basin-wide circulation of the Marmara Sea and to relatively isolate the Erdek, Bandırma, and İzmit Bays. Aydoğdu et al. [10] investigated the circulation of the sea by using the Finite Element Sea-Ice Ocean Model (FESOM), offering realistic atmospheric forcing, for 6 years. This long-term simulation allowed them to analyze the combined response of the Marmara Sea to atmospheric forcing and strait dynamics. The results showed the annual mean wind fields (which are northeasterlies) and the annual mean of current velocity in the sea. According to this study, the general movement of the surface waters was westward in the sea and served as an outflow in İzmit Bay. Ilıcak et al. [11] used a high-resolution unstructured finite element grid model to simulate the Turkish Strait System (TSS), using realistic atmospheric forcing and lateral open boundary conditions. The System of Hydrodynamic Finite Element Modules (SHYFEM) was customized and ran for 4 years. The model captured the well-known basin-wide ocean processes, e.g., the buoyant jet coming from the İstanbul Strait into the Marmara Sea via the surface; the anticyclonic gyre in the center of the Marmara Sea, which occurs due to the jet; the cold intermediate layer at the halocline depth; and the relatively higher salinities found in the bays.

İzmit Bay, which is 50 km long and 2 to 10 km wide in a west-to-east orientation, has a distinctive topographic shape (Figure 1). It consists of three basins: eastern, central, and western. The eastern basin has a maximum depth of 30 m and connects with the central basin via a narrow strait. In the central basin, there are 2 deep regions (160 m and 200 m) close to the southern coast, which has a steep slope. The central and western basins are connected by a narrow and short strait (the Hersek Delta) at a depth of about 50 m. The western basin is about 50 m deep. It deepens towards the Marmara Sea and reaches a depth of 200 m [12–14]. As a part of the Marmara Sea, İzmit Bay contains distinct water masses in terms of physico-chemical aspects [15–18]. Although it displays two-layer stratification, such as partially or salt-wedged estuaries, these layers are not riverine and marine, but rather both are of marine origin. Low-salinity water of Black Sea origin constitutes the upper layer, whereas high-salinity Aegean water forms the lower layer [13]. Thus, İzmit Bay is hydrographically distinct from typical estuary habitats. Salinity in the upper layer varies in a wide range of 21–32 ppt throughout the year, while variation in the lower layer is within a narrower range of 37.5–38.5 ppt [15]. As a part of the Marmara Sea, an intermediate layer forms between layers and the density variation between layers ( $\Delta\rho/\rho \approx 10^{-2}$ ) is quite high [2,13]. The circulation in the bay, on the other hand, depends on two main drivers: differences in sea level between the bay and the Marmara Sea and the atmospheric conditions of the region [19]. The differences in sea level occur (i) due to the influx of the Black Sea waters via the İstanbul Strait; (ii) tidal amplitude, ranging between 8 to 10 cm; and (iii) northeast–southwest wind [20]. Winds, especially severe ones, are significant drivers of the bay's dynamics since they not only affect the circulation patterns but also cause vertical mixing between the upper and lower layers at shallow depths [12–14,19]. Ergül [18] stated that wind speed and directions are important factors in preventing the occurrence of a very thin upper layer and near-surface hypoxia in İzmit Bay. Furthermore, it is suspected that meteorological conditions could be the reason for the unexplained massive fish mortalities that are reported on occasion from the region. Altıok et al. [14] studied the diurnal variation in stratification seen in İzmit Bay using in situ temperature

and current velocity data, investigating the influence of atmospheric conditions. This study, based on high-frequency buoy measurement in a 2-layer system, found that the bay was quite dynamic since severe northern and southern winds reduced the stratification and increased the stirring between the layers. The response of the bay to the wind was rapid, while the time delay between the beginning of the strong winds and the highest interface depth was calculated to be nearly 82 h (~3.4 days).

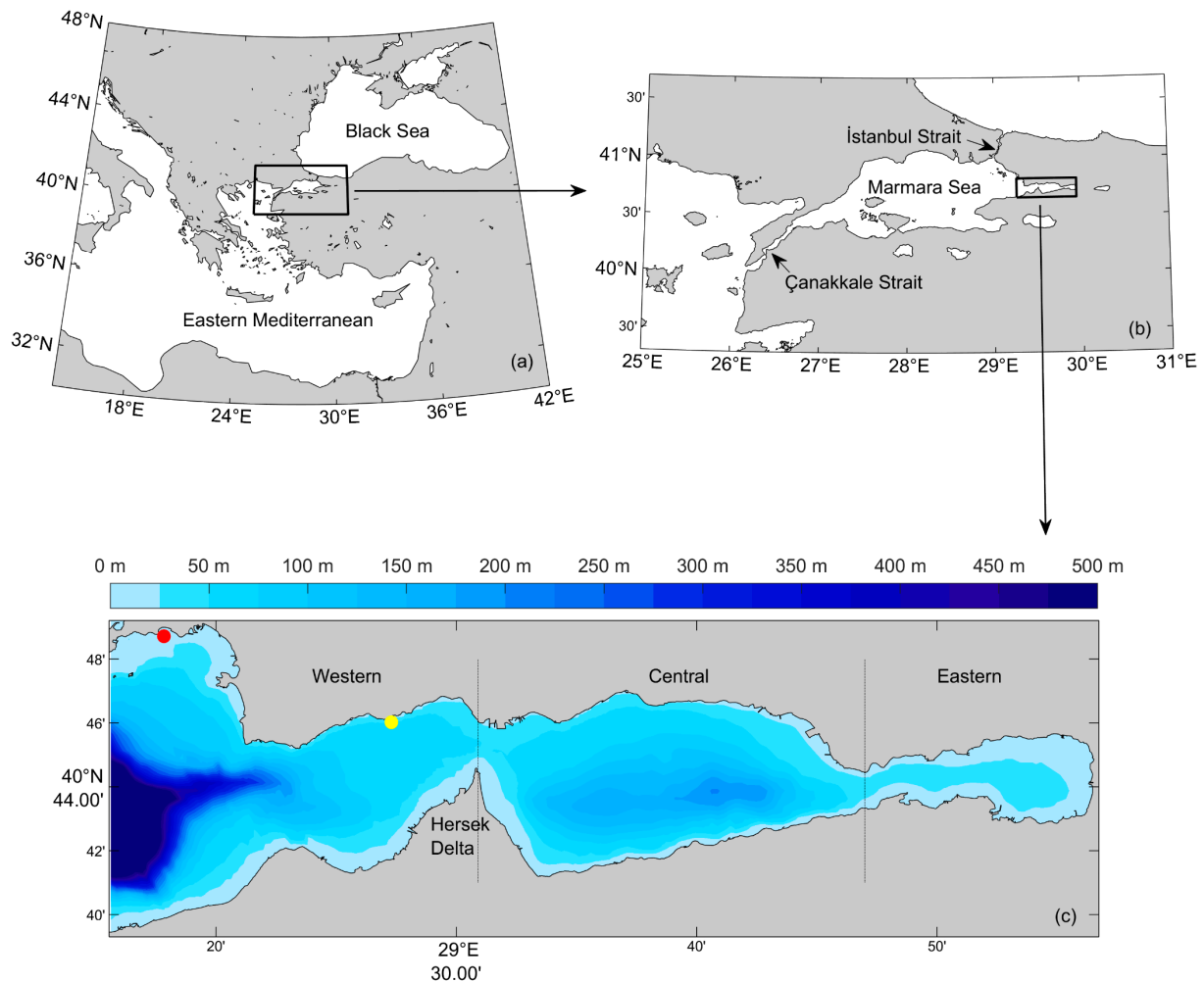


**Figure 1.** (a) The Marmara Sea connects the Black Sea to the Eastern Mediterranean via the İstanbul and Çanakkale Straits; (b) İzmit Bay is located at the easternmost edge of the Marmara Sea. (c) Due to its distinctive topography, it consists of three basins: western, central, and eastern basins. The red and yellow dots are the location of the weather station and the buoy, respectively. (Bathymetry: GEBCO, 2020 [21]).

All the efforts to assess the circulation of İzmit Bay, mentioned above, were highly significant to pollution studies. Taymaz et al. [22] determined mercury, cadmium, and lead levels in water, sediment, and fish samples taken from the bay. Baştürk et al. [12] identified the pressures of the bay, i.e., the types and amounts of pollution, and the chemical oceanographic characteristics, assimilation capacity, and nutrients that limit primary production. Tuğrul et al. [23] provided some findings on water quality and on wastewater loads and their sources. Their study also mentioned water's biochemical and physical characteristics based on data obtained both from previous studies and measurements performed from May 1984 through to April 1985. The levels of polycyclic aromatic hydrocarbons (PAH) and polychlorinated biphenyls (PCBs) were measured in seawater, sediment, and mussels as part of the research in [24,25]. Ünlü and Alpar [26] aimed to determine the concentration of

the PAHs in the surface sediments of the bay. In their study, they stated that the inflow of two distinct water masses has a significant effect on sediment transportation and deposition in the bay. After the 1999 earthquake in İzmit Bay, a condition of anoxia was noted as a result of heavy loads of industrial waste and the presence of a lot of sink debris at the bottom of the bay [17,27]. During the mucilage event (October 2007–February 2008) in the Marmara Sea, İzmit Bay also suffered from intense mucous formation (slippery aggregates). Tüfekçi et al. [28] investigated the composition and abundance of phytoplankton and the corresponding environmental conditions during this event in the Marmara Sea by focusing on İzmit Bay. Tolun et al. [29] highlighted the significance of performing home wastewater treatment based on an integrated coastal zone management strategy to avoid the water quality of the bay declining. According to Ergül [30], nutrients from the resuspension of sediment after northeastern storms served as fuel for phytoplankton reproduction. Ülker et al. [31] built a circulation model using 20 years of the ECMWF's operational archive data with a  $0.10^\circ$  horizontal resolution and evaluated 36 oil spill scenarios in the bay. Kavzoglu and Goral [32] investigated the performance of five water quality indices to effectively map mucilage aggregates that occurred from May to July 2021 on the sea surface in the bay. Additionally, they mentioned how the general and wind-driven circulation affected the movement of mucilage during the event, causing mucilage to accumulate in the bay.

Wind has several significant impacts on ocean dynamics, particularly at the surface, by generating waves; influencing the exchange of heat, moisture, and gases between the atmosphere and the sea; causing turbulence and the mixing of water masses; creating surface currents through frictional drag; and triggering vertical movements of water, known as upwelling and downwelling. Previous studies have shown that that are wind-driven effects in nearshore waters as well. Wang [33] examined nontidal circulation in the Chesapeake Bay, where there were large wind-driven fluctuations occurring at several-day time scales, and demonstrated the influence of wind on upstream salt intrusions. Monismith [34] presented a solution for the response of a rectangular n-layered, stratified lake to an arbitrarily varying level of wind stress and compared their calculations with measurements made in the Wellington Reservoir. Drinkwater [35] studied the response of an open, stratified bay to wind forcing. The wind-induced response of St Georges Bay was investigated based on current and temperature measurements. It was found that cross-bay wind stresses produce Ekman drift, with compensating flow in the lower layer near the entrance to the bay, and that the near-bottom currents are coherent, with along-bay wind stresses in the interior. Llebot et al. [36] proposed a conceptual model of the physical behavior of a shallow (6 m deep) micro-tidal estuary (Alfacs Bay). They found that bay–sea exchange rates decrease significantly in the strong wind scenarios and that the magnitudes of these changes are largely dependent on wind direction. Lips et al. [37] investigated wind-driven circulation and related oxygen and nutrient dynamics in the Gulf of Finland in winter and observed that strong and sufficiently long-lasting estuarine upwind events caused the collapse of vertical stratification and the development of a barotropic flow system consisting of outflow. Lai et al. [38] explored the estuarine circulation variation in the Pearl River Estuary in response to the different tidal and wind forcing conditions. Their model experiment showed that the circulation is determined by the mixing intensity seen during the spring tide, and that the wind has less influence than this; however, during the neap tide, the mixing is weaker, and the circulation can be dramatically altered by the wind-induced current. Mazoyer et al. [39] demonstrated the important impact of hydrodynamic-driven processes (which are Mistral, easterly winds and offshore water intrusions) on the dispersion of contaminants within the semi-enclosed bay of Toulon. In this study, we examined the direct effect of wind on circulation, as in the studies mentioned above. On the other hand, wave-induced processes, like Stokes drift, 3D radiation stress, vortex force, and wave-breaking-induced near-shore circulation in coastal bays, lagoons, inlets, and lakes, are also noteworthy, as described in [40–44].

In brief, for more than 40 years, İzmit Bay has attracted the attention of marine scientists interested in both circulation and pollution studies. Since the prevailing wind is a major driving force behind current variability in such coastal waters and has positive or negative impacts on water quality by creating dynamic or stagnant conditions, we investigated the wind-induced response of İzmit Bay by adopting the method of process-oriented hydrodynamic modeling. We also aimed to examine the salinity, temperature, and current variances occurring due to the wind's direction, speed, and duration while taking topography factors into account. For this reason, the ocean circulation model was customized for the bay and several numerical experiments were carried out to examine the sensitivity of the bay's circulation for 8 different wind sectors and 6 conditions of gradually increased wind speed.

## 2. Materials and Method

### 2.1. Observation Data

Current measurements were taken seasonally in the east–west direction or vice versa in 2018 and 2019, following the vessel traffic lane in the bay. The vessel-mounted 150 kHz Ocean Surveyor ADCP (Acoustic Doppler Current Profiler, Teledyne RD Instruments, San Diego, CA, USA) was set to a 2 m bin size to collect data along the water column. The depth of the first bin was 8 m relative to the transducer depth and the blanking distance. This, unfortunately, caused the most wind-sensitive surface of the sea to be missed during the measurements. For the velocity reference during the processing of the data, the bottom track option was selected along with the ending profile “BT Depth” and the “Cos(BeamAngle)” option on the WinADCP v1.14, ADCP processing software. Since the measurement line along the bay was quite long, ensembles were averaged to 5 min. However, this increased the unmeasured area due to side-lobe interference at the bottom. Because of all the disadvantages described above, current measurements alone were not sufficient to determine the circulation. On the other hand, these measurements were used to validate modeling studies and gave hints about hydrodynamics of the bay.

To examine the model's performance, temperature and salinity data obtained from an automatic profiling buoy (APB5, SAIV A/S, Bergen, Norway) were also used. The buoy was deployed in the summer of 2018 at 29.455° E–40.767° N within the framework of the “Integrated Marine Pollution Monitoring 2017–2019 Program” by the Republic of Türkiye's Ministry of Environment, Urbanization and Climate Change and TÜBİTAK-MRC. It was programmed to measure between 0 to 45 m daily. The accuracy rates of the sensors are  $\pm 0.002$  °C and  $\pm 0.003$  ppt for temperature and salinity, respectively. The location of the buoy was quite close to the northern shore of the western basin; however, it was at a total depth of 50 m, which was enough to monitor both layers of the Marmara Sea (Figure 1c). A measurement performed on 23 September 2018 was used to define the first 45 m of the initial conditions in the simulations.

In addition to marine data, we obtained an observational wind dataset from the Turkish State Meteorological Service (TSMS). All weather stations in the bay were located onshore and almost all of them were sensitive to local conditions e.g., high buildings, trees, distance from shore, high altitude of the station, and so on. For the modeling study, the data obtained from Tuzla Breakwater Weather Station were preferred since the station was far enough away from adverse local atmospheric conditions to allow us to measure the weather conditions of the sea accurately.

Data captured between 2016 and 2021 were selected in order to analyze the recent conditions of the bay. According to the wind rose shown in Figure 2, the NE sector is the dominant wind direction in the region, with 37%. In addition, the speed range of 6–10 m/s was observed mostly from the NE direction, with 10.5%. (Figure 3).

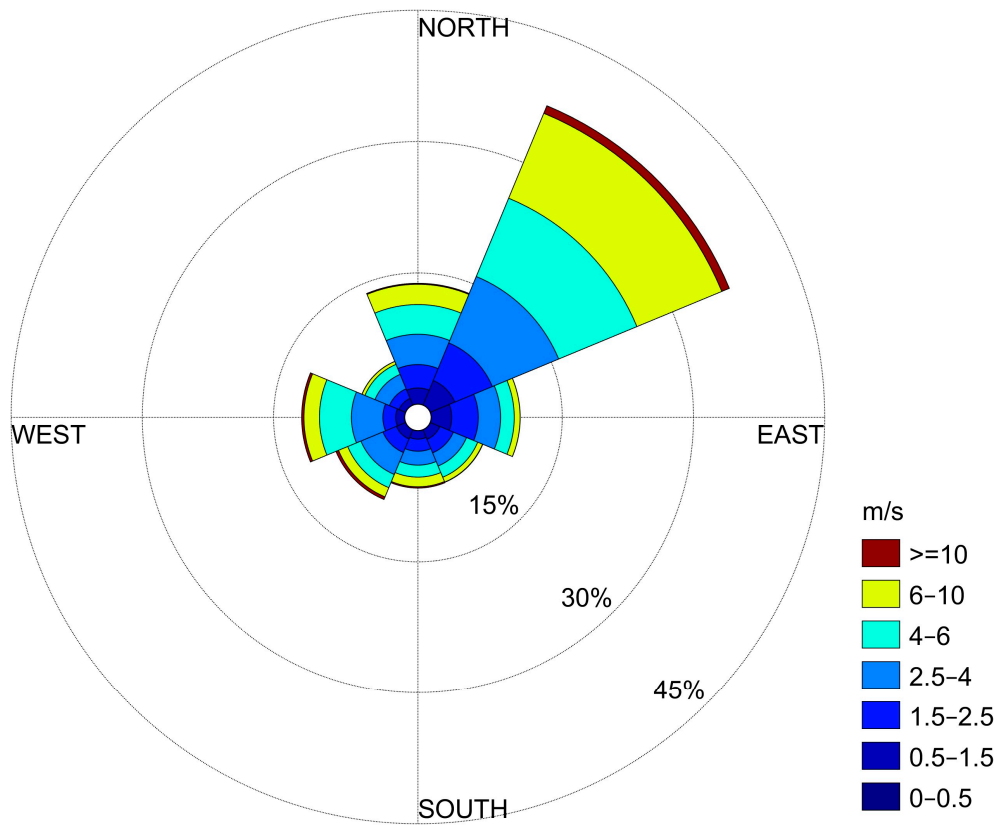


Figure 2. Wind rose of the data (2016–2021) obtained from Tuzla Breakwater Weather Station.

		%							
		0-0.5	0.5-1.5	1.5-2.5	2.5-4	4-6	6-10	>=10	
DIRECTION	N	13.8	0	1.8	2.7	3.5	3.4	2.3	0.1
	NE	37	0	3	4.6	8.2	9.7	10.5	0.9
	E	10.2	0	2.3	3	2.5	1.6	0.7	0
	SE	6.5	0	1.2	1.7	1.6	1.4	0.6	0
	S	6.6	0	0.9	1.4	1.6	1.4	1.1	0.1
	SW	8.6	0	1.1	1.7	2.7	1.6	1.1	0.3
	W	11.8	0	1	1.5	3.6	3.7	1.8	0.3
	NW	5.4	0	0.8	1.2	1.8	1.2	0.4	0
TOTAL		0.2	12.3	17.7	25.5	23.9	18.4	1.8	
TOTAL			0.2	12.3	17.7	25.5	23.9	18.4	1.8

Figure 3. Heat map of the data (2016–2021) obtained from Tuzla Breakwater Weather Station.

The wind data were applied to the following series of processes to categorize wind speeds in the simulations.

- Wind speeds below 0.5 m/s were accepted as “calm” and removed from the observed data.
- Wind speeds were grouped by eight wind directions (cardinal and ordinal winds) and were sorted in ascending order.
- Wind speeds were clustered, corresponding to the percentiles of 10, 25, 50, 75, 90 and 99.
- Average wind speeds were taken for each percentile.

The results are given in Table 1.

**Table 1.** Wind speeds (m/s) corresponding to percentiles in 8 wind directions and percentile means.

Percentiles/Directions	N	NE	E	SE	S	SW	W	NW	MEAN
10%	1.3	1.6	1.1	1.1	1.2	1.3	1.6	1.2	1.3
25%	2	2.8	1.5	1.7	1.9	2.1	2.7	1.9	2.1
50%	3.4	4.5	2.3	2.8	3.3	3.3	3.9	3	3.3
75%	5.3	6.5	3.7	4.4	5.3	4.8	5.3	4.2	4.9
90%	6.9	8.2	5.4	5.9	7.3	7.6	7	5.5	6.7
99%	9.7	10.8	8.2	9.1	11.9	11.9	11.2	8.3	10.1

### 2.2. Model Description

In addition to in situ measurements, we carried out numerical experiments, using the ocean circulation model in order to investigate the response of the bay to the wind. Here, we used the Massachusetts Institute of Technology general circulation model (MITgcm), which is a primitive equation ocean circulation model designed for the study of a wide range of scales in both the ocean and atmosphere [45,46]. The MITgcm is a z-coordinate finite-volume model that solves incompressible Navier–Stokes equations on an Arakawa-C grid using Boussinesq approximation. The articles [45,47] provide a detailed description of the model formulation, which includes implicit free surface and partial step topography.

In this study, MITgcm was customized to meet the features of İzmit Bay, with particular attention paid to the forcing acting on it. The hydrostatic version of the model was implemented even though the horizontal resolution of the domain was  $0.0013^\circ \times 0.001^\circ$  ( $\approx 103 \text{ m} \times 111 \text{ m}$ ). Parkan [48] compared the hydrostatic and non-hydrostatic versions of MITgcm, which were taken from the study of Sannino et al. [9]. It was concluded that using a non-hydrostatic model does not bring significant improvements in terms of either temperature, salinity distribution, or the circulation pattern in the Turkish Strait System. As a result, we selected hydrostatic runs for the study. The bathymetry for the model domain was based on gridded data from the General Bathymetric Chart of the Oceans GEBCO\_20, which has a resolution of 15 arc seconds [21]. No-slip conditions were imposed at the bottom, and so were lateral solid boundaries. The quadratic bottom drag coefficient ( $C_d$ ) was set equal to 0.02 and was dimensionless. Horizontal and vertical viscosity coefficients were also constant and were chosen as  $A_h = 0.2 \text{ m}^2\text{s}^{-1}$  and  $A_z = 1.5 \times 10^{-5} \text{ m}^2\text{s}^{-1}$ , respectively. The diffusivity coefficients of temperature and salinity were the same, but  $K_h = 0.02 \text{ m}^2\text{s}^{-1}$  and  $K_z = 2 \times 10^{-5} \text{ m}^2\text{s}^{-1}$  were chosen for the horizontal and vertical ones. Similar to the numerical experiments of [9,48], a third-order direct space-time (DST) flux-limited scheme was chosen for the tracer advection operator. A modified UNESCO formula [49] was selected as the equation of state used to calculate the density of the ocean.

The shallow-water regime was defined as the moment where the surface and bottom Ekman layers overlap and interfere [50]. Shallow-water regimes can be up to 50 m in terms of total water depth in coastal oceans. According to the ADCP measurements, water below a depth of 60 m was observed to be stagnant in the bay. Therefore, the model had 32 equal z-levels, where thicknesses were 2 m. Below a 64 m depth, the thickness value was 8 m. A higher vertical resolution was preferred at the upper part since it was the most wind-sensitive part of the water column. The wind stress values for each direction in the simulations were calculated using the function named “windstress.m” [51]. In the study of Kämpf et al. [52], all simulations began with a state at rest, and the wind speed was linearly increased from zero to a constant value over the first simulation day (ramping day) to avoid the generation of unwanted gravity waves. After the first day of the simulation, the domain was forced with a constant and spatially uniform wind speed for 10 more days, since Tilburg [53] explored wind-driven near-shore circulation on subinertial timescales of up to 10 days. It is also known that the passage of cyclonic systems in the winter months affects the Marmara Sea for periods of 3 to 12 days [20].

Kämpf et al. [52] used the method of process-oriented hydrodynamic modeling to demonstrate the effects of short-lived wind events around the reef islands of the tropical Pa-

cific Ocean. The same method (process-oriented hydrodynamic modeling) was customized to İzmit Bay to investigate the response of the bay to wind and its sensitivity to direction and speed. Therefore, all the work was conducted by external forcing, i.e., the wind [54]. To ensure there was no available potential energy at the beginning of the simulations, the temperature and salinity profiles were laterally and homogeneously derived from in situ data, representing the late summer conditions of the bay (Figure 4).

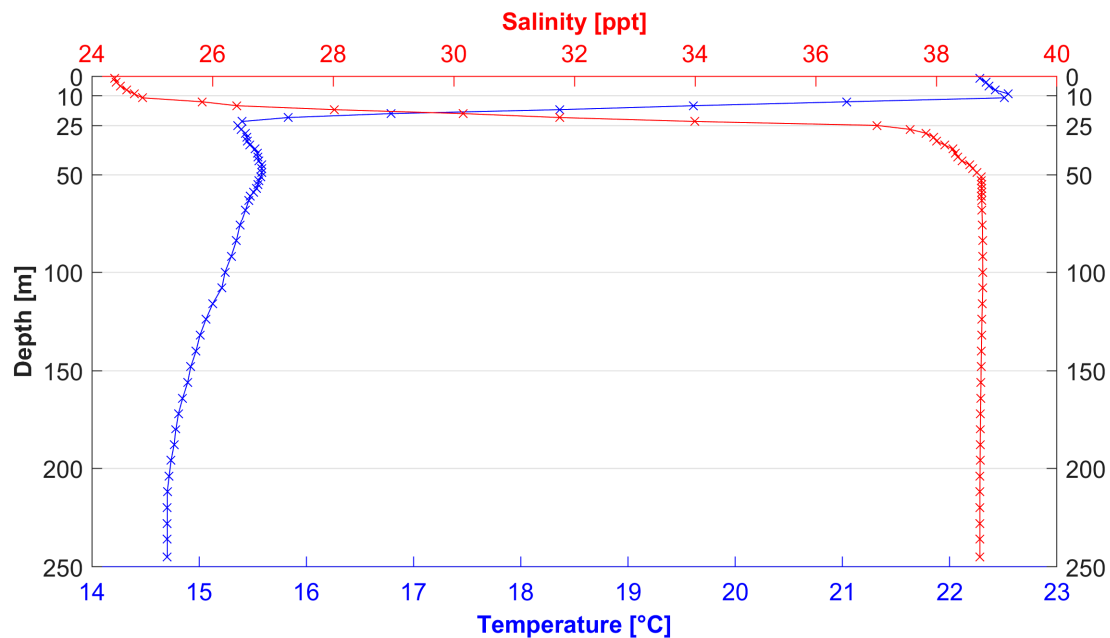


**Figure 4.** Initial conditions of the numerical simulations for temperature and salinity, based on in situ data collected during the “Monitoring the Water Quality and Terrestrial Inputs in İzmit Bay and Developing Suggestions for Preventing Pollution” project.

Two MITgcm packages (in version 67r) were activated in the simulations. The first one was the turbulent closure scheme K-profile parameterization (KPP) [55], which was used to model vertical sub-grid-scale mixing. The second one was the OBCS package (open boundary conditions for regional modeling), which is fundamental to regional ocean modeling with MITgcm. Since many details must be considered in regional ocean modeling, MITgcm accommodates many possible options for the users. Among these options, Orlanski-BC [56] was selected due to the lack of actual lateral boundary conditions, although its handicaps were known from coastal studies [57]. However, this option was considered to be better than using a closed boundary on the west side of the domain. The Marmara Sea is not large enough to generate its own tide [58]. Hence, it was assumed that there was no significant tidal forcing on the open boundary of the bay. To avoid sea level rises because the bottom counter current was overstated by the model, we enabled the balance routine in order to balance transport through open boundaries. This routine computed the net flow across the boundaries, obtaining zero net inflow. The model was also set to recompute divergence after the pressure solver step to ensure the conservation of the volume of free surface solution.

### 2.3. Model Validation

The current measurement, collected on 9 August 2018, was selected for use in simulation validation against observational data. When the strong northeast wind dominated the region, the average wind speed reached 11 m/s. (Figure 5a). A counter-current at 10 m depth was observed, even though the wind direction was favorable for the transportation of water masses out of the bay (Figure 5b). This questionable current condition was best simulated at the end of 72 h in the NE 10.1 m/s simulation (Figure 5c). This was also

in close agreement with the response time ( $\sim 3.4$  days) values calculated in the study of Altioik et al. [14]. On the other hand, the simulated velocities were underestimated due to the higher horizontal viscosity coefficient, which was increased to avoid instabilities near the lateral boundary on the west side of the domain (Figure 5d). Besides this compromise, the results of the simulations were satisfactory since they were also in good agreement with the other studies mentioned in the introduction.

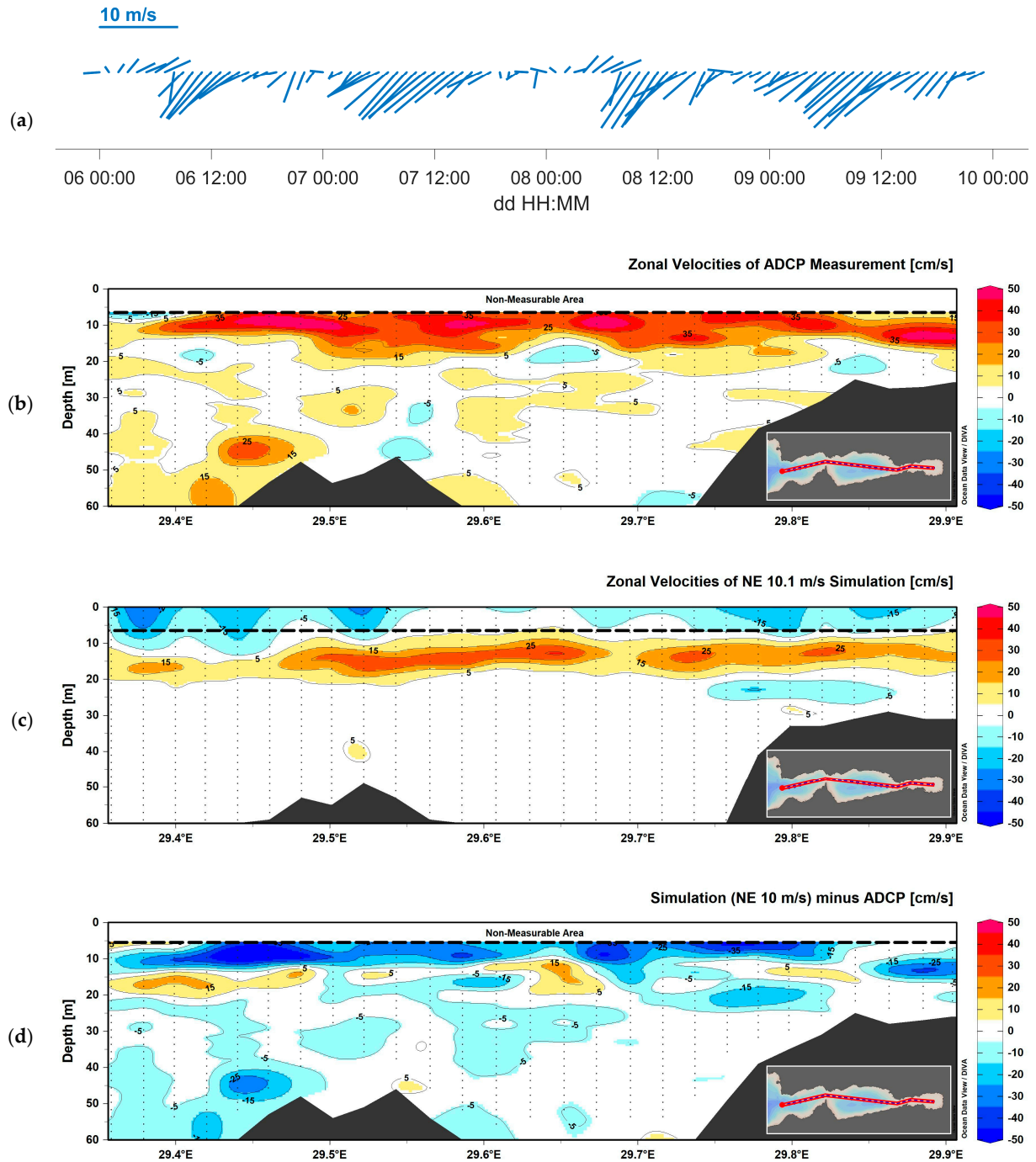


**Figure 5.** (a) Hourly wind velocities, measured at Tuzla Breakwater Weather Station. (b) The zonal component (U) of the current measurement conducted on 9 August 2018. The upper part of the water column was unmeasured due to the depth of the current profiler mounted on the vessel and the blank distance after transmission. (c) The zonal velocities at the end of 72 h in the NE 10.1 m/s simulation. (d) Difference between NE 10 m/s simulation and ADCP measurement.

At the end of the summer of 2018, the buoy captured a rise in the lower layers when the prevailing wind was northeasterly, with an average speed of 6 m/s (Figure 6a). This wind event dominated the bay for about a week and changed the thermohaline structure, with a thinner upper layer, an increase in surface salinity, and a decrease in surface temperature (Figure 6b,c). The upper layer was so thinned that the initial depth of the lower layer was about 5 m on 29 September 2018. On the other hand, an NE 6.7 m/s simulation performance was sufficient to capture the thermohaline changes at the buoy's location. In the simulation, the upper layer becomes thinner, but not as much as observed. This is probably due to the higher horizontal viscosity coefficient, which we increased to avoid instabilities near the lateral boundary on the west side of the domain. This also causes the largest bias along the water column, which appears around the halocline (5–20 m). Additionally, below 15 m, the observed temperature is always higher than the simulation results. This is due to the lack of information at the lateral boundary. The root-mean-square error values for salinity and temperature are 1.43 ppt and 0.42 °C, which are acceptable under adiabatic forcing and Orlanski–BC conditions.

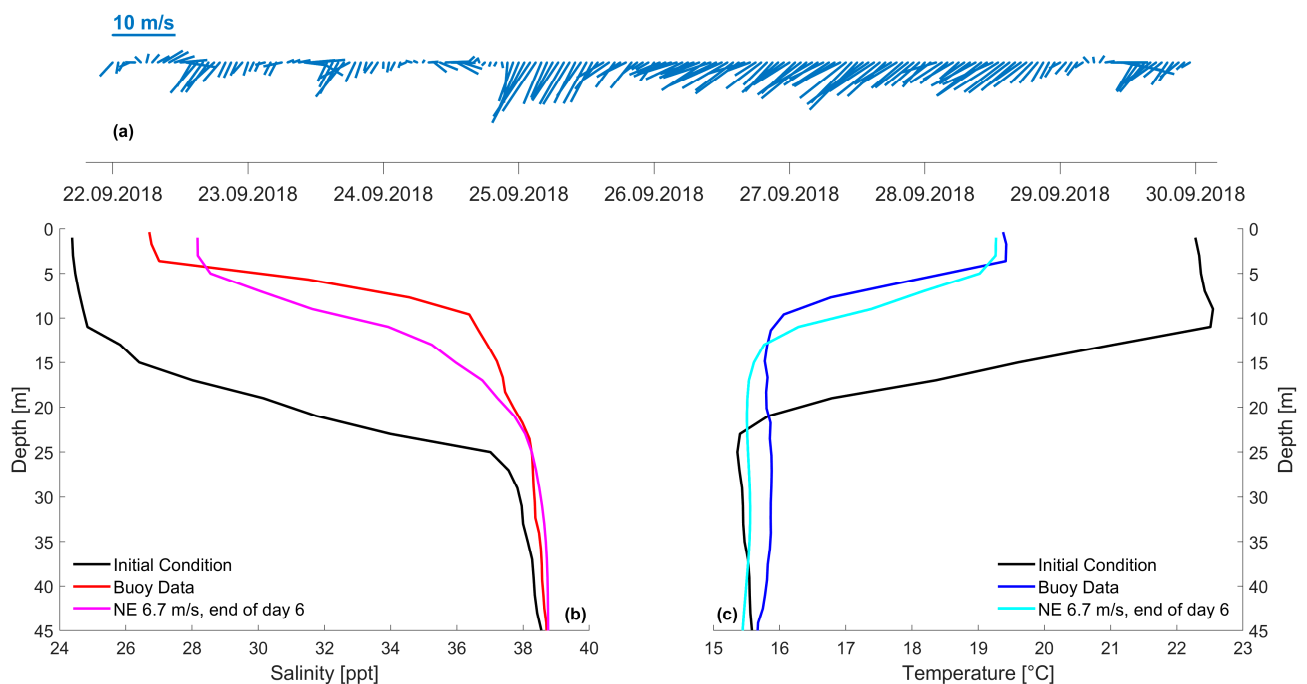


**Figure 6.** (a) Hourly wind velocities, measured at Tuzla Breakwater Weather Station. (b) Salinity and (c) temperature profiles of simulations for initial conditions derived from the buoy data on 23 September compared with the buoy data on 29 September and the NE 6.7 m/s simulation result at the end of 6 days, excluding ramping day.

### 3. Simulation Results

We performed 48 simulations under adiabatic conditions at the air–sea interface for the eight directions and six speeds in order to analyze the sensitivity of the bay. In this section, the temperature ( $T$ ) and salinity ( $S$ ) profiles of the simulations are analyzed at the deepest point of the central basin. Since the variations in physical parameters ( $T$ ,  $S$ ) below 60 m depth are negligible, only the first 60 m is shown in Figure 7. We also investigated the temporal response of the surface at the same point while including all directions on polar diagrams (Figure 8). Figure 9 shows spatially averaged temperature and salinity values of simulation results and their differences with the initial conditions. In addition, we showed surface conditions where the wind speed was 6.7 m/s, as the upwelling in the eastern basin was more pronounced at this speed than others (Figure 10). Next, the temporal change in salinity was examined to comprehend the upwelling and downwelling processes of the

eastern basin (Figure 11). Finally, the response of the bay along the thalweg line is shown in the upper 60 m in Figures 12–14.

### 3.1. *T and S Profiles of the Central Basin*

Due to diffusion between layers, all thermoclines and haloclines weaken in all simulations (Figure 7). In conditions of light and gentle breeze (1.3, 2.1, and 3.3 m/s), diffusion is the primary process as thermohaline variations from the initial condition occur in clines and surface changes are minor. The effect of strong winds (4.9, 6.7, and 10.1 m/s), on the other hand, becomes noticeable depending on their speed and direction. The surface currents induced by the winds having positive zonal components (i.e., NW, W, and SW) converge eastward in the bay, resulting in a deeper upper layer. The maximum increase in upper-layer depth (from 10 m to 30 m) is simulated for the southwesterly wind using 10.1 m/s forcing. On the contrary, the surface layer drifts westward due to the winds having negative zonal components (i.e., NE, E, and SE), resulting in different thermohaline properties via upwelling and vertical mixing. The most drastic change in the upper layer is obtained under NE 6.7 m/s forcing. Surface salinity increases to 32 ppt, while surface temperature decreases to 17 °C. The final results of E 6.7 m/s and E 10.1 m/s simulations are also noteworthy, as the surface temperature is 18 °C and the salinity is 31 ppt in the central basin.

The drastic changes mentioned above occur due to the combination of upwelling and mixing processes. However, in NE 10.1 m/s and SE 10.1 m/s simulations, the wind stirring in the upper layer dominates, and only mixing the process changes the thermohaline properties of the upper layer. Surface salinity increases to 29 ppt and 30 ppt and surface temperature decreases to 19 °C and 18.5 °C, respectively. In NE 4.9 m/s, N 6.7 m/s, N 10.1 m/s, and S 10.1 m/s simulations, weaker upwellings and vertical mixings increase the surface salinity up to 27 ppt and decrease the surface temperature up to 20 °C. The reason behind this is that NE 4.9 m/s is not strong enough to create hydrodynamics as strong as those NE 6.7 m/s and NE 10.1 m/s produce. N and S sectors are also crosswinds for the bay.

### 3.2. *Physical Variations of Surface Responses to Wind*

Figure 8 shows the surface salinity and temperature changes during the simulation period for stronger winds at the central point of the bay. The figures that show the response of the weak winds are given in Appendix A. The response of the surface increases with the duration and intensity of the forcing. Surface salinity is always increasing with the duration of the NE 6.7 m/s forcing, especially after 5 simulation days. The increase in surface salinity in the NE 6.7 m/s simulation is also always greater than the increase observed in the NE 4.9 m/s simulation. However, the direction of the wind and the shape of the bay also play important roles in the response. While there is no change in surface salinity and temperature in the SW 6.7 m/s simulation, the maximum change is achieved in the NE 6.7 m/s simulation. This is the most obvious example showing the effect of wind direction and its polarity (NE–SW direction) on the surface parameters in the bay. There are also exceptions to the above results. The maximum changes in temperature and salinity are obtained in NE 6.7 simulations rather than NE 10.1 m/s simulations. This is due to the bay's narrow passages, which restrict surface waters leaving the bay, and the lateral boundary definition in the west, which creates surface countercurrents in order to balance the water budget. Additionally, the polarity of the surface changes shifts from the NE–SW direction to the E–W direction since the maximum and minimum changes are achieved in the E 10.1 m/s and W 10.1 m/s simulations, respectively.

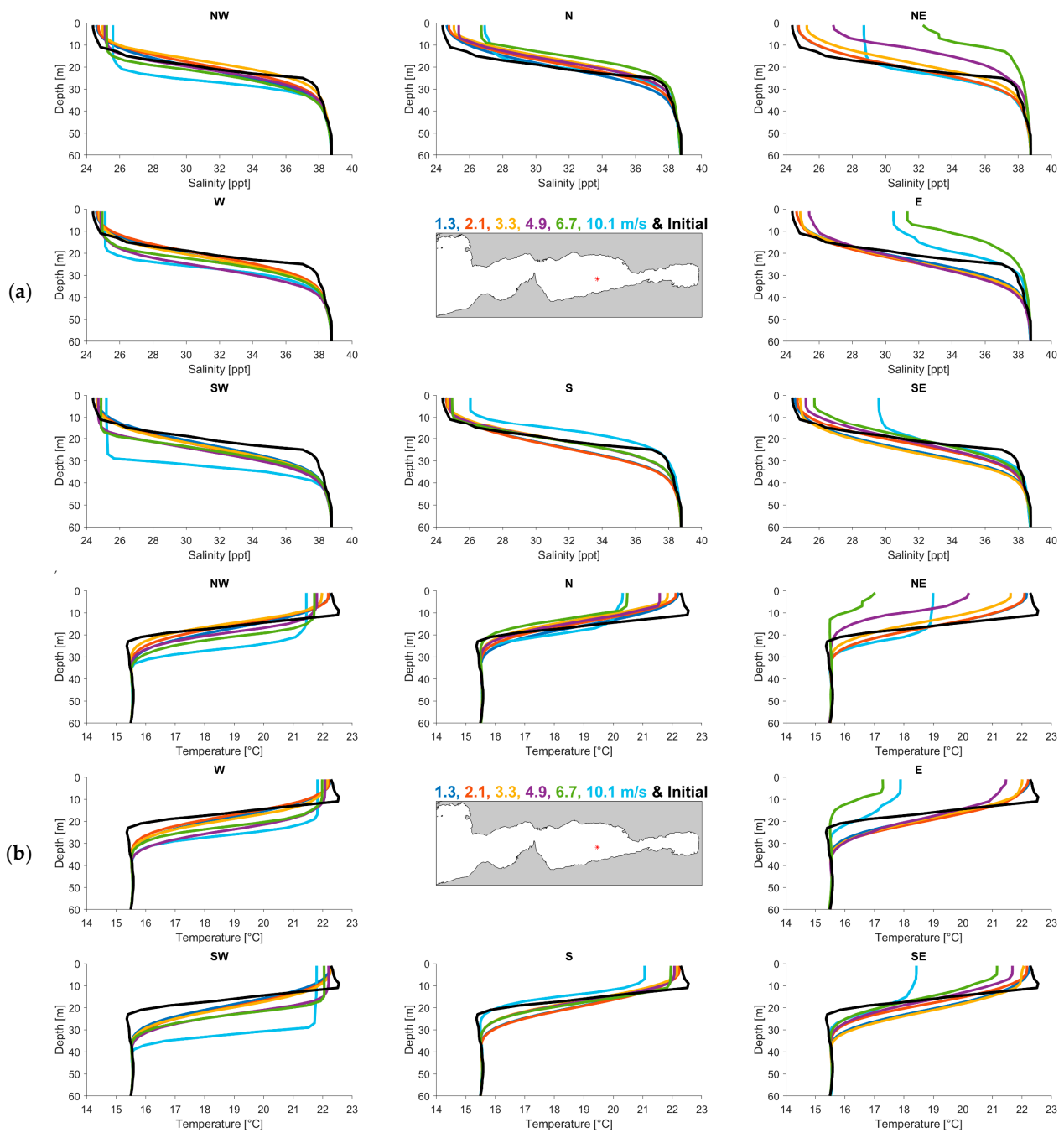


**Figure 7.** Profiles of salinity (a) and temperature (b) in the central basin after 11-day runtime with the initial conditions.

The surface temperatures, salinities, and current velocities of the simulations after the 11-day run are given in Figure 9. In each sub-table, the simulation results for that variable are given according to the direction, shown on the left, and the speed, given at the top. In the top 2 rows, spatially averaged surface temperature ( $T_{s,mean}$ ) and salinity ( $S_{s,mean}$ ) values, as well as the minimum surface temperature ( $T_{s,min}$ ) and the maximum surface salinity ( $S_{s,max}$ ) in the bay, are presented and colored according to their values. The differences from the initial values (22.3 °C and 24.4 ppt) are also calculated and are given in the following two rows below. In these rows, negative and positive changes are colored in blue and red bars, respectively. In the bottom row, spatially averaged speeds of zonal currents ( $U_{s,mean}$ ) and their maximum values ( $U_{s,max}$ ) are presented in

green data bars. When the speed of wind is less than or equal to 2.1 m/s, the changes in surface temperature and salinity are negligible since the maximum differences are  $-0.6\text{ }^{\circ}\text{C}$  and 0.8 ppt, respectively. In cases where the average zonal speeds are lower than 5 cm/s, the bay can be considered stagnant. At the speed of 3.3 m/s forcing, some noticeable changes are obtained in minimum temperatures and maximum salinities; however, the basin-wide effect is still insignificant. Therefore, wind speeds equal to or less than 3.3 m/s are considered weak winds for the bay.

When the speed is 4.9 m/s, the physical changes in the bay become more distinctive depending on the wind direction. In the NE 4.9 m/s simulation, the average surface temperature and salinity changes are  $-1.8\text{ }^{\circ}\text{C}$  and 2.2 ppt, while the changes in the opposite direction, that is, in the SW and at the same speed, are  $-0.1\text{ }^{\circ}\text{C}$  and 0.2 ppt, respectively. The most drastic variations in surface temperature and salinity are achieved in the NE 6.7 m/s simulation. At the same speed, SW forcing still causes the mildest changes in surface parameters. The reason for this is that the wind's direction governs whether there is an outflow at the upper layer, resulting in upwelling and the formation of a new water mass at the layer, or an inflow at the surface, resulting in the upper layer piling up in the east. Even though the forcing, i.e., wind speed, intensifies, the changes in surface parameters do not increase that much. This is due to the limiting factors, which are the shape of the bay, the particularly narrow passages, and the open lateral boundary, reflecting the outflow into the bay.

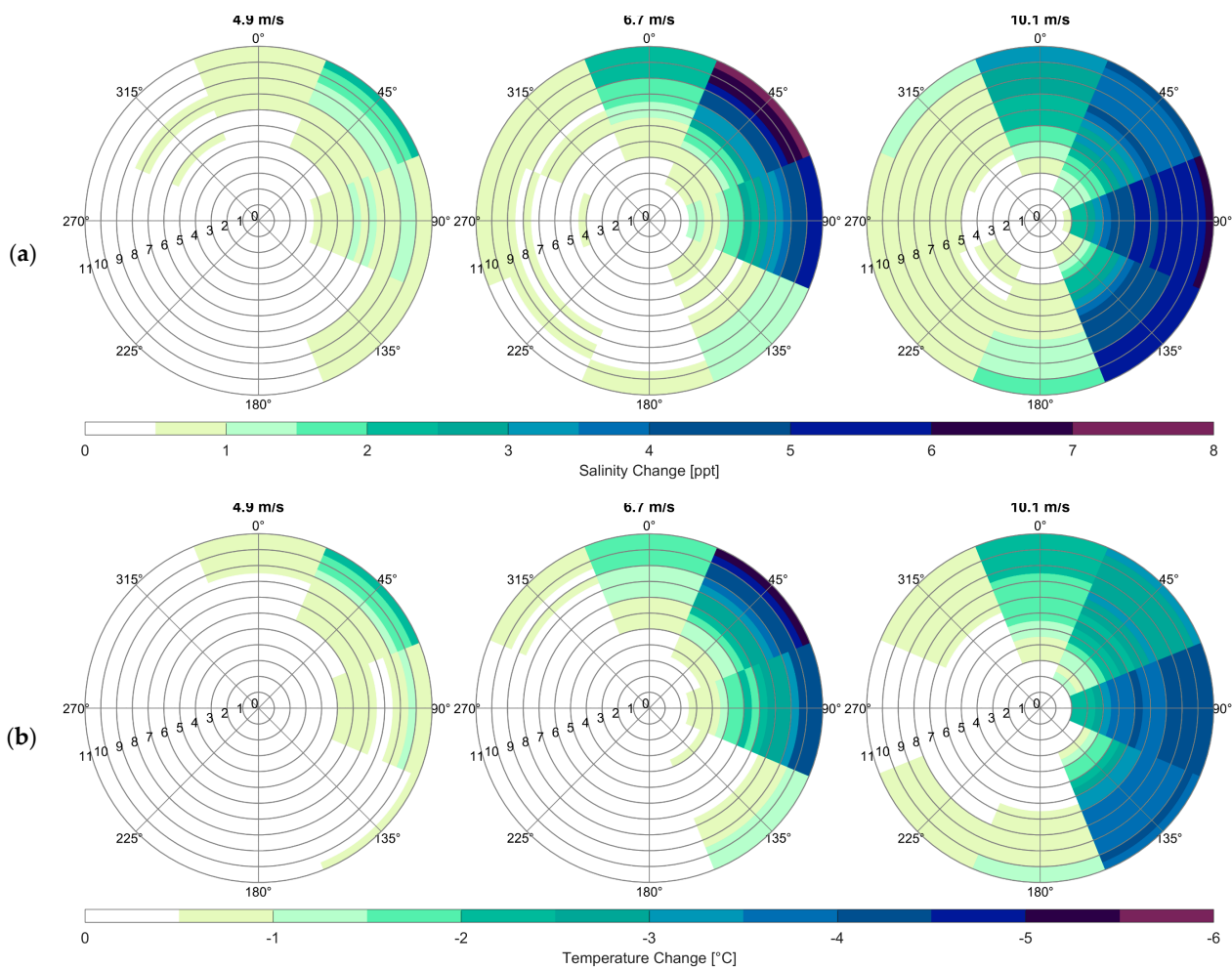


**Figure 8.** Surface salinity (a) and temperature (b) changes of the central basin based on wind direction sectors for corresponding strong wind speed simulations (4.9, 6.7, and 10.1 m/s). Inner circles represent 11 simulation days.

### 3.3. Surface Circulations of 6.7 m/s Wind Forcing

Of the 6 wind speeds, the 6.7 m/s simulations produced the most notable results. As shown in Figure 9, the largest decrease in surface temperature and the largest increase in surface salinity occurred in the 6.7 m/s simulations. Therefore, in this and the following sections, we examined the 6.7 m/s simulation results.

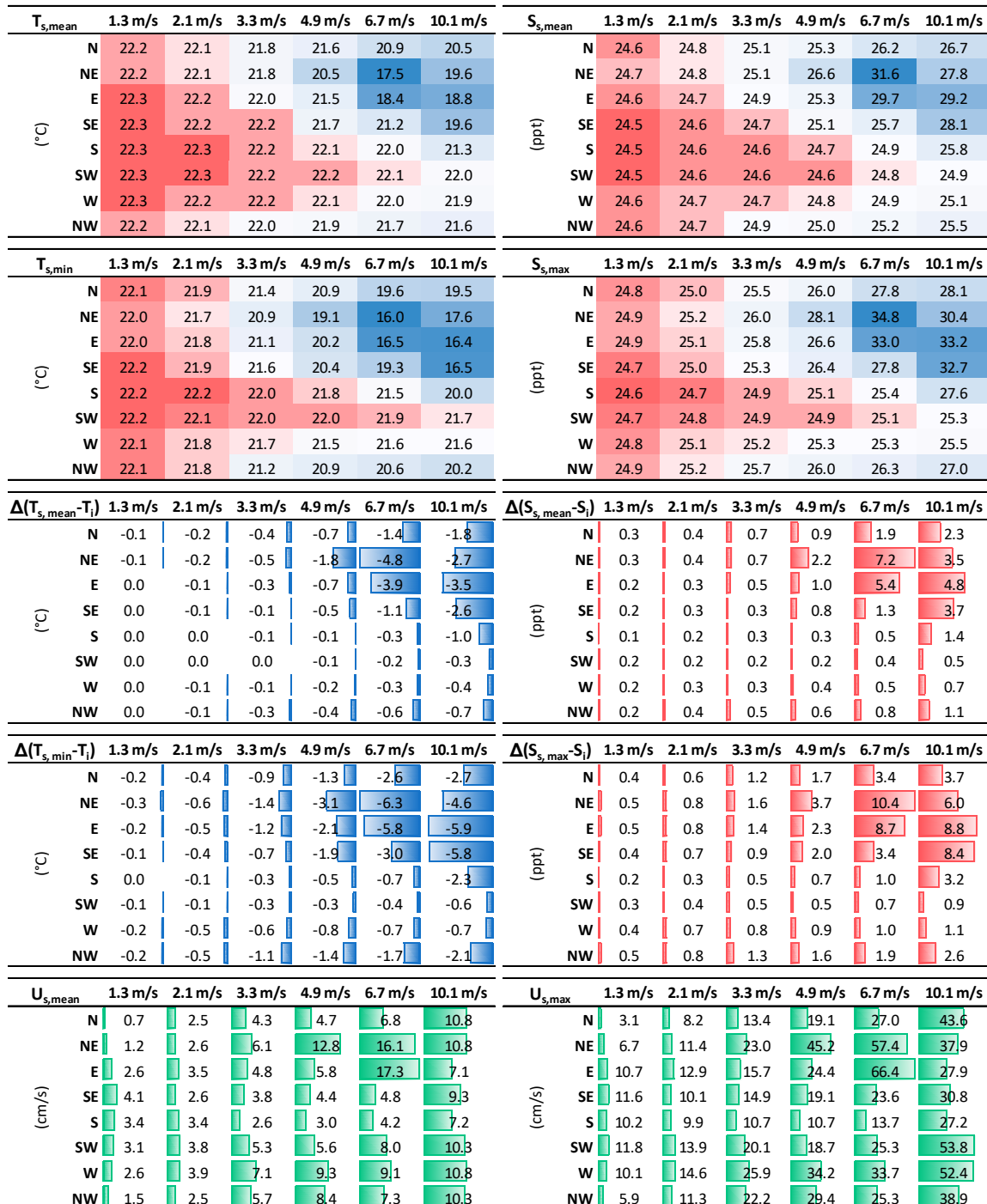
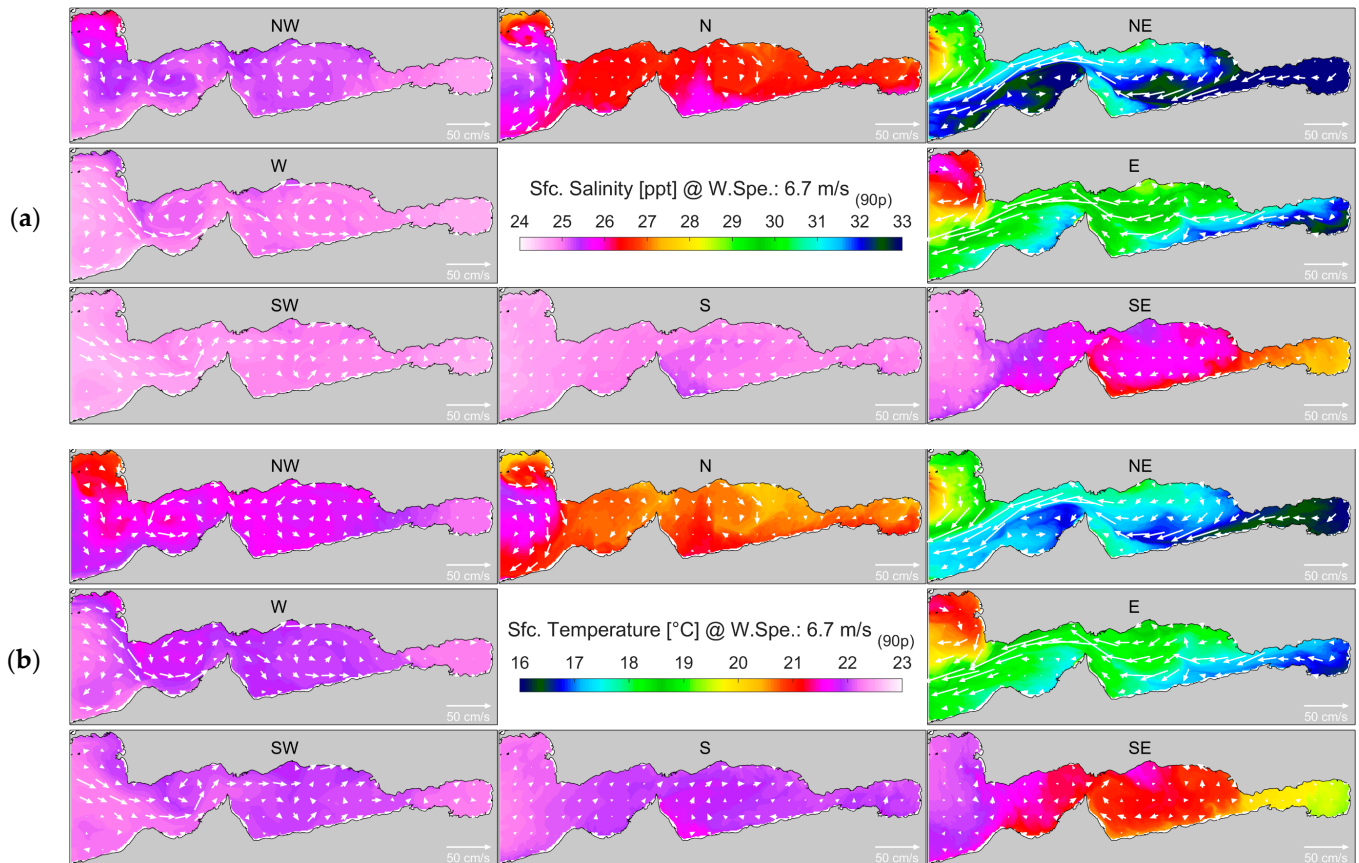


Figure 9. Surface parameters at the end of simulations and their differences from the initial conditions.

Figure 10 shows the current regime and hydrographic characteristics (T, S) of the surface under a wind speed of 6.7 m/s. The polarity of the response for the wind sectors is seen over the whole bay since the surface salinity, temperature, and dynamics are significantly different between NE and SW forcing. NE wind drags the surface waters out

of the bay, generating a jet with upwellings along the shores of the south coast and at the most eastern part. In the SW 6.7 m/s simulation, wind-driven transport occurs towards the eastern part of the bay. The surface set up in the bay causes the deceleration of the inflow. There are also topographically steered cyclonic eddies in the western and central basins. Therefore, the surface currents in the SW 6.7 m/s simulation are slower than the surface currents in the NE 6.7 m/s simulation.



**Figure 10.** Surface salinities (a) and temperatures (b) of simulations of forcing with a 6.7 m/s wind speed after 11-day runtime.

The coastal jet driven by the NE and E directions plays a significant role in overturning the circulation of the bay and transforming the mass of the upper-layer water by producing several upwelling zones along its path. These upwelling zones along the bay cause higher salinities and lower temperatures at the surface, even under adiabatic forcing. The jet follows the southern coast of the bay from the east coast to the western basin. Due to the narrow passage at the Hersek Delta, the jet is forced to the northern coast in the western basin. While outflowing the bay, the jet approaches the south coast again. Since it reaches the Marmara Sea, it is also expected that the alongshore jet will affect the sea by transporting the physicochemical properties of the upper layer [27]. In the absence of such a strong coastal jet, for example in the SE 6.7 m/s simulation, surface temperature and salinity changes are milder compared to those seen when the jet forms and are limited to the eastern basin.

In addition to the simulations described above (NE, E, and SE), the N 6.7 m/s simulation also ends up altering the physical parameters (T, S) of the surface. The variations in surface parameters seen in the N simulation are smaller than the variations in the NE, E, and SE simulations, with the mixing covering almost the whole bay. On the other hand, although the S direction also has a cross-bay wind like N, the response is completely different, as the variations are negligible, and the zonal currents are the slowest among the

6.7 m/s speed simulations. This is due to the combination of downwind currents and the Coriolis force; this results in a quasi-outflow (inflow) for N (S) in the surface layer. In the westerly component wind simulations (SW, W, and NW), changes in surface parameters are also negligible, as wind-induced surface currents produce inward-flowing currents in the surface layer and the thermohaline definition of the lateral boundary. These inflows are also topographically steered, resulting in cyclonic eddies in the western and central basins.

Since the eastern basin had the most significant response compared to other basins at the wind speed of 6.7 m/s, we also investigated the temporal response of the relevant basin. The intermediate layer (where the salinity is 31 ppt) deepened at the end of NW, W, and SW simulations (Figure 11). At the beginning of the simulation, the intermediate layer was 20 m in depth. However, it deepened to 21 m, 22 m, and 25 m, respectively. In the S simulation, the intermediate layer remained the same, but in the N simulation, the center of the layer rose to 15 m depth. Then, upper-layer mixing commenced while the risen layer remained at its new depth after the seventh day of simulation. In the SE simulation, the intermediate layer remained at the same depth, while stronger upper-layer mixing occurred. NE and E simulations were significantly different than the others since the intermediate layer reached the surface at the end of 8 and 9 days, respectively. These responses to the NE and E directions were obviously due to Ekman transport to the west and resulted in upwelling in the basin. A similar process was identified on 6 November 2015 in the previous study related to the bay [30]. After long-term northeastern gusts (35 km/h, ~9.7 m/s for 5 days), an upwelling occurred and resulted in sediment resuspension. The other significant finding was that the surface salinity increases greater than the winter salinity values. Thus, the upwelling in the basin explained why the salinity in the upper layer varied in a wide range of 21–32 ppt throughout the year [15].

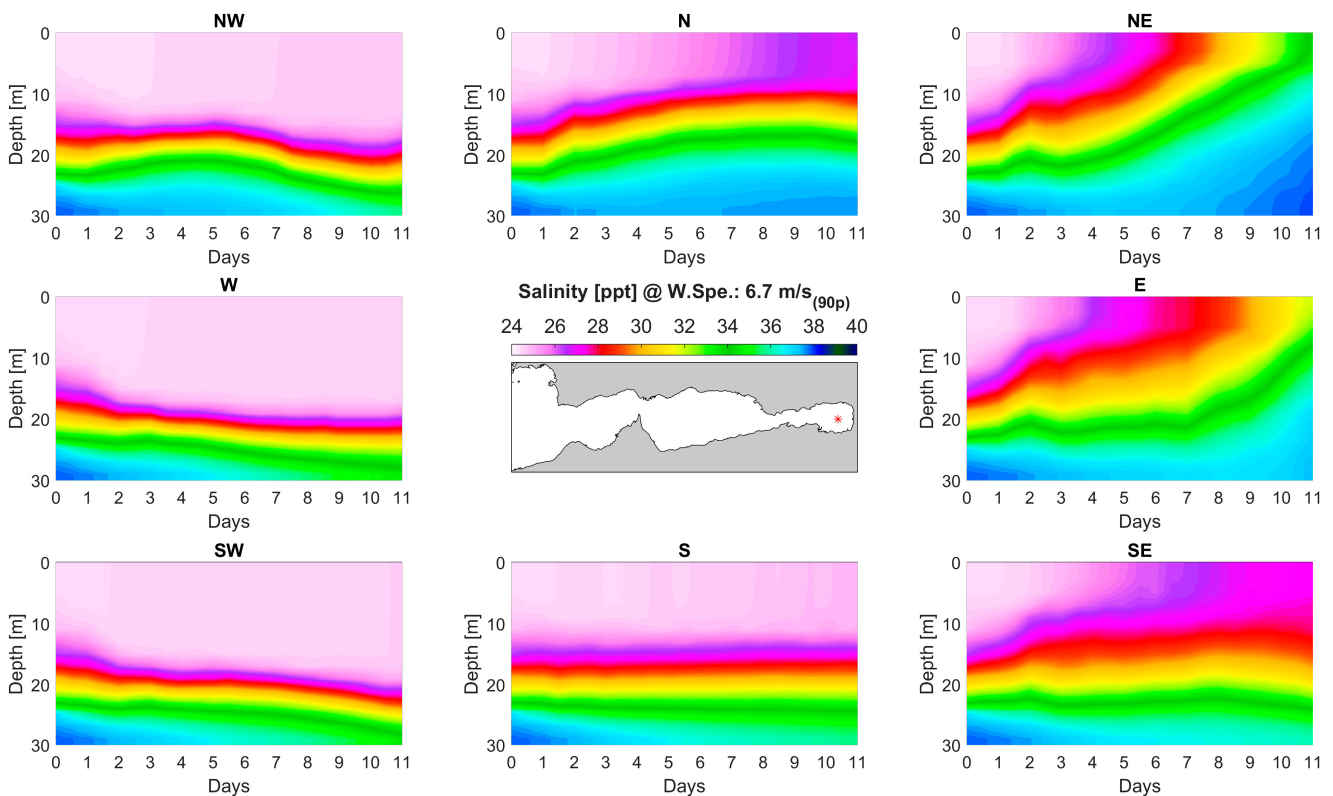


**Figure 11.** Variation of salinities in the eastern basin during the simulation period of forcing with a 6.7 m/s wind speed.

### 3.4. Results of the 6.7 m/s Forcing along the Thalweg Line

The salinities, temperatures, and zonal velocities along the thalweg line under the forcing of 6.7 m/s wind speed are shown in Figure 12, Figure 13, and Figure 14, respectively. Zonal velocities are also shown to define variations in temperature and salinity since the domain is forced adiabatically.

The significant changes obtained after the 11-day simulation are as follows: In the eastern basin, a water mass with the same temperature and salinity values as the initial condition is obtained in NW, W, and SW simulations. However, the mixing layer depth is increased since the western component winds tend to cause downwelling at the innermost point. In the central and western basins, wind mixes surface waters vertically and creates shear-flow instabilities at the base of the upper layer. Below 20 m depth, topographic interactions become effective, in addition to the processes mentioned above. As seen in Figure 13, the depth of the 18 °C isotherm increases at 29.5° longitude where the Hersek Delta sill is located.

In N and S simulations, the depth of the 18 °C isotherm remains the same along the thalweg line, but it is higher in the N simulation than in the S simulation. The variation in physical parameters in the N simulation is also greater than seen in the S simulation. This is because of the weak surface transportation caused by the Coriolis effect. In the N simulation, the base of the upper (mixed) layer rises to a 10 m depth, which leads to more shear instabilities. At the lower layer, the water mass is still stagnant at the end of the S simulation, while an internal wave in the central basin is generated by overflow on the Hersek Delta sill at the end of the N simulation.

In NE, E, and SE simulations, when the constant wind speed is 6.7 m/s, the responses to the wind forcing are significantly different than other scenarios since upwelling becomes dominant in the bay. The upper layer is transported towards the west (Figure 14), outside of the bay, and this leads the layers below the upper layer to rise along the water column. At the end of the NE simulation, the upper layer is completely transported outside of the bay. The 34 ppt isohaline rises to 10 m depth along the thalweg, with strong mixing between 29.4 ° and 29.5 ° longitudes (west of the Hersek Delta), and the same pattern also occurs in the eastern basin (Figure 12). This layer also reaches the surface due to upwelling at the most eastern coastline. A similar process was defined by Chiggiato et al. [8] as the large displacement pycnocline depth that occurs due to the storm-driven upwelling/downwelling dynamics associated with northeasterly winds. The other noteworthy result is the rise in the lower layer in the western basin. This rise creates an overflow over the Hersek Delta sill towards the central basin. This overflow causes disturbances in the lower layer and leads to an internal wave with an amplitude of approximately 15 m. At the end of the E simulation, a similar response to the N simulation is obtained. The rise in the 34 ppt isohaline remains below a 10 m depth and the amplitude of the internal wave in the central basin lower layer is 10 m. At the end of the SE simulation, lateral stratification occurs from the surface up to 20 m depth. The surface temperature cascades from 22 °C to 19 °C along the west–east direction. Below 20 m, the stratification specific to the Marmara Sea remains without any significant disturbance. This is due to the lack of strong transport of the upper layer to the outside of the bay. Instead, there is an outflow from the central to the western basin of the Hersek Delta sill.

In short, of the 48 simulations, the 6.7 m/s simulations show us how important the wind direction can be, because the coastal jet, upwelling, downwelling, interlayer mixing, overflow events, and peak changes in surface temperature and salinity are simulated at this speed.

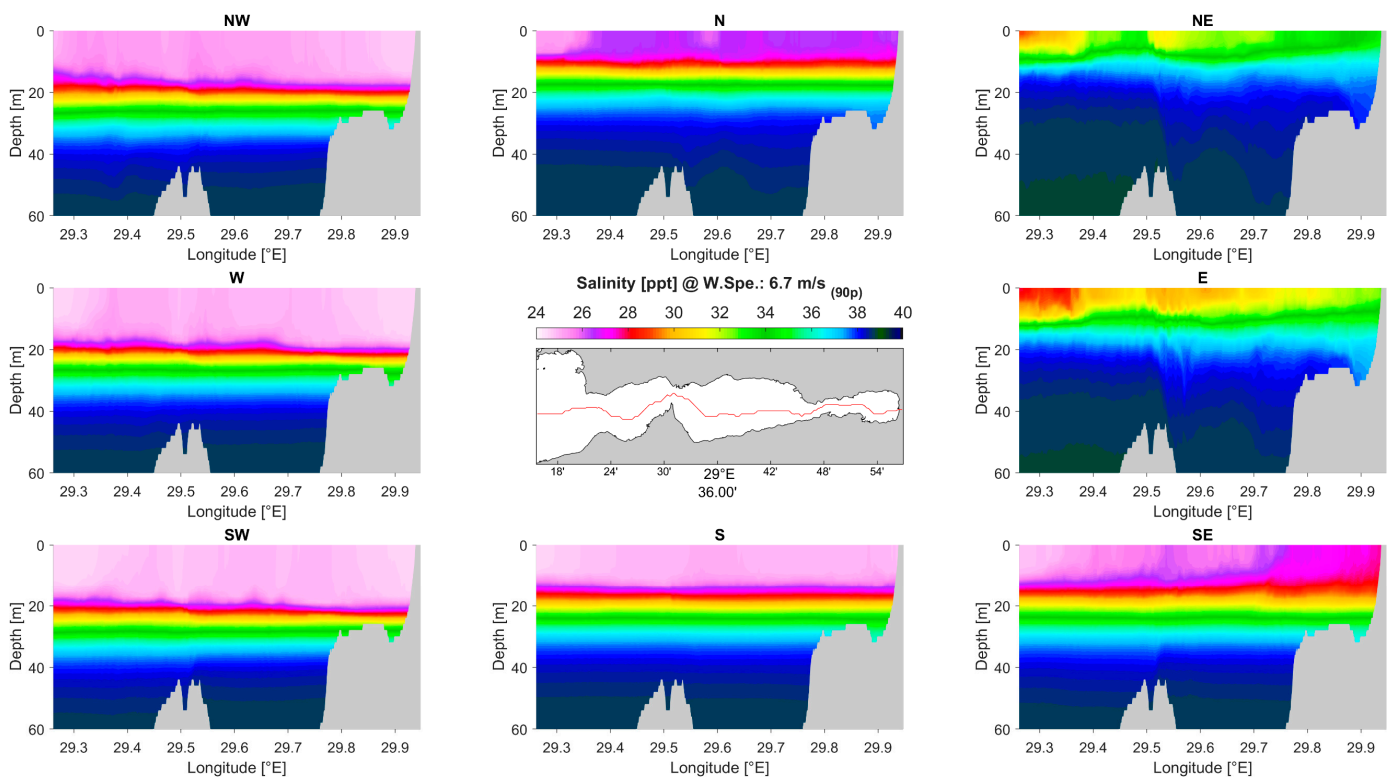


**Figure 12.** Salinities along the thalweg line at the end of the 11-day simulation of forcing with a 6.7 m/s wind speed.

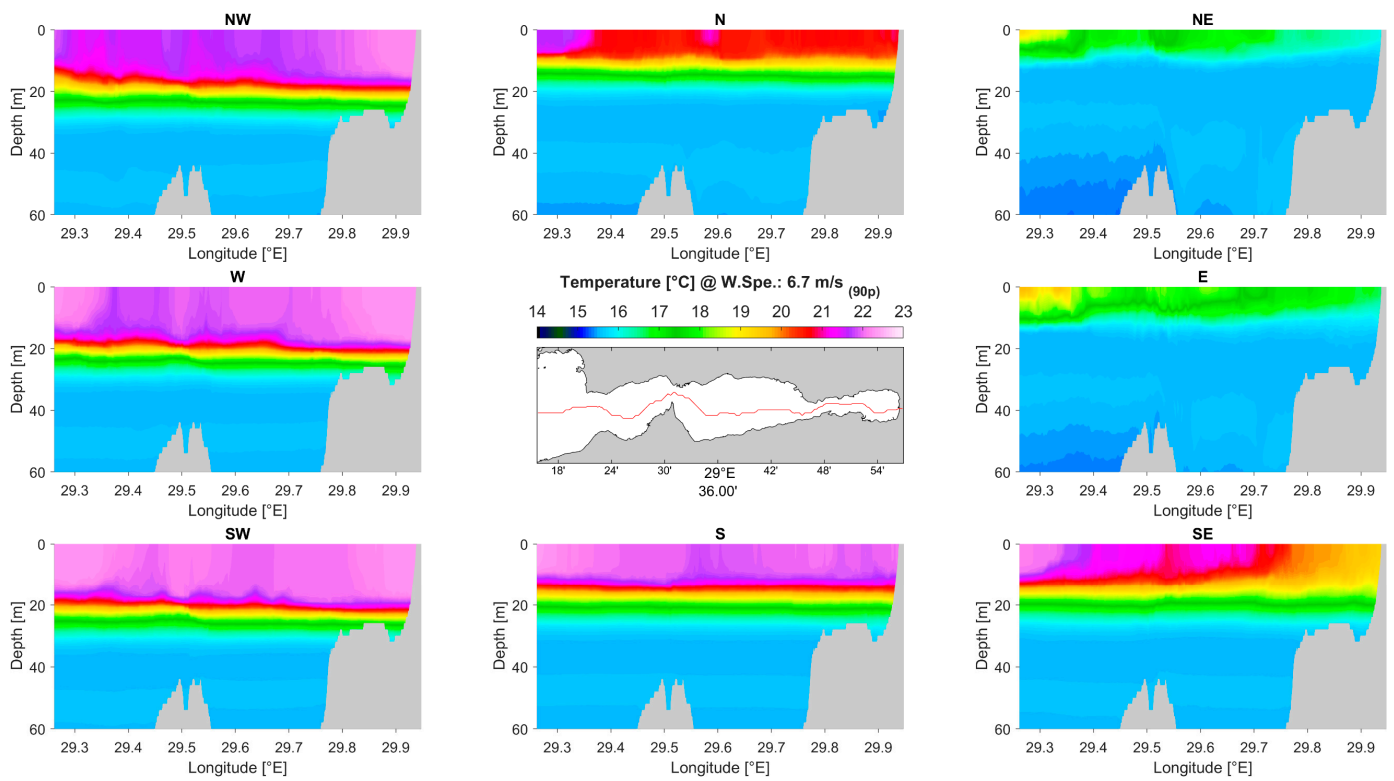


**Figure 13.** Temperatures along the thalweg line at the end of the 11-day simulation of forcing with a 6.7 m/s wind speed.

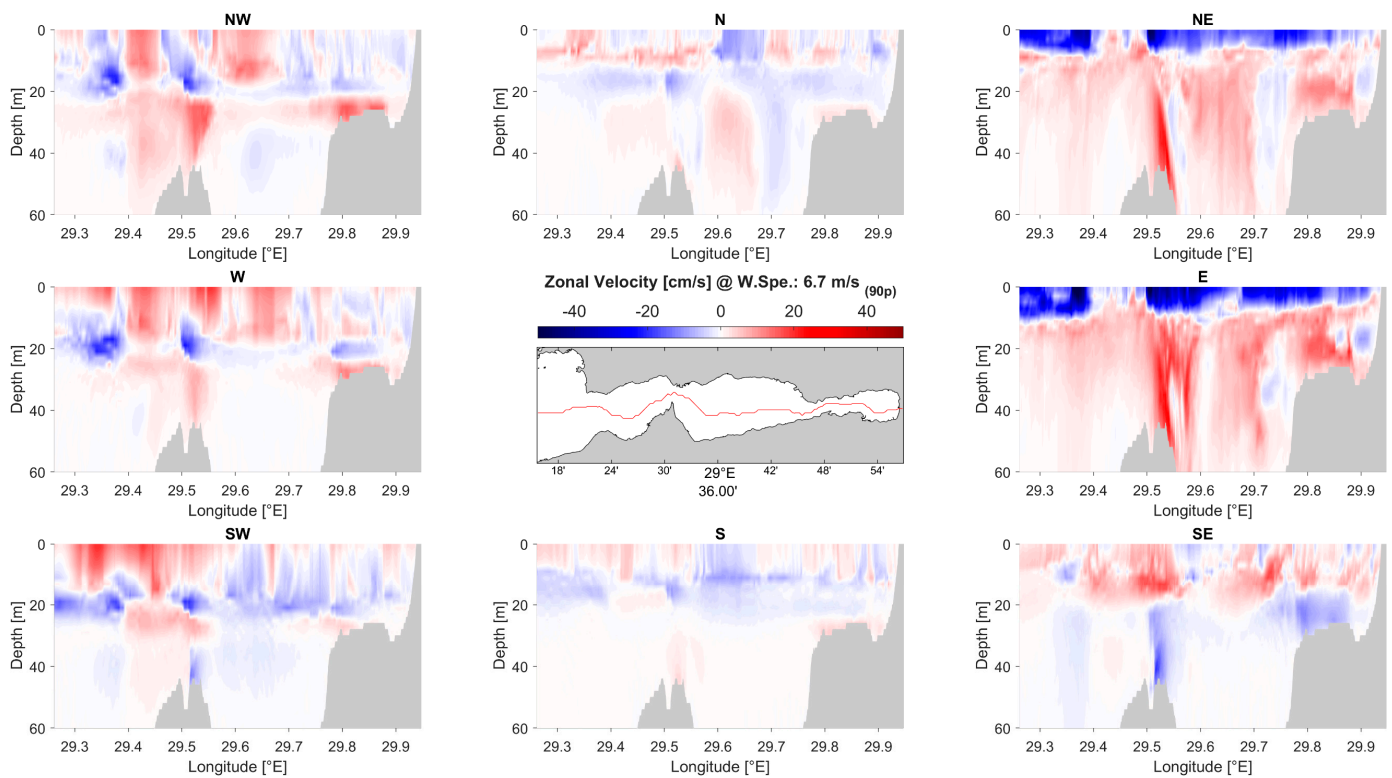


**Figure 14.** Zonal velocities along the thalweg line at the end of the 11-day simulations of 6.7 m/s wind speeds.

#### 4. Discussion and Conclusions

In this study, we investigated the sensitivity of İzmit Bay to the wind, which was one driver of the region [19,20]. We first classified wind speeds based on measurements obtained from the weather station on the Tuzla Breakwater. In addition, we built up a regional ocean circulation model by customizing the MITgcm based on previous studies [9,15,48]. Since we employed process-oriented hydrodynamic modeling [52], we omitted all forcing factors except for wind stress [54]. We considered all wind directions, analyzing more speeds than previous studies [16,19] in order to examine all responses that were never considered before. The simulations were initiated at a state of rest and the forcing was gradually increased to the idealized wind speeds to avoid unwanted gravity waves. The runtime of the simulations was 11 days, the optimum runtime required to balance computational costs and obtain distinctive model results. For the initial condition, a late summer measurement was preferred in order to also study the effect of wind on temperature and salinity variations during stormy weather conditions. The results of 48 adiabatic simulations are limited to the first 60 m of depth due to negligible changes below 60 m.

The conditions of İzmit Bay were simulated under weak wind speeds (1.3, 2.1, and 3.3 m/s): the bay remained stagnant or became quasi-stagnant. Since the bay is always under serious anthropogenic pressures, the stagnancy of the bay under calm or weak wind conditions can stimulate the deterioration of the water quality by keeping the pollutants and nutrients in the bay [12], leading to hypoxia or worse [18], eutrophic conditions, mucous formations, and accumulations [28], heavy metal loads in sediment and biota [22], and longer recovery time after any environmental disaster [17].

In terms of stronger wind speeds (4.9, 6.7, and 10.1 m/s), the influence of wind forcing is more pronounced depending on its direction. The winds with the west component (onshore winds) cause the convergence of the upper layer towards the east, resulting in a deeper upper layer. In addition, the winds with the eastern component (offshore winds) induce the transportation of the upper layer outside the bay by generating a coastal jet

with an approximate speed of 50 cm/s. This coastal jet, which is simulated for the first time, constitutes upwelling zones, breaks the permanent stratification, causes water mass transformation, and creates an overturning circulation in the bay. The most remarkable upwelling event is simulated under conditions of NE 6.7 m/s forcing because surface temperature and salinity variability reach the maximum level. Even though the forcing was adiabatic between air and sea, the water mass was transformed to become more saline at the upper layer and accelerated towards the west—out of the bay. Altıok et al. [14] described these mixing processes under strong winds as a decrease in buoyancy frequency and the dominance of the shear leading to mixing. The response of the bay under the strong northeasterly forcing is also coherent with the findings of [8,10] regarding the displacement of the pycnocline and the response of the Sea of Marmara to the wind. Additionally, the numerical results demonstrate that dynamical interactions are primarily responsible for the abrupt cooling (up to 5 °C) that occurs during strong wind events, one of which was observed by Tuğrul et al. [23]. During the scientific expedition of [23], surface salinity was measured at 24 ppt on 13 February 1975. After 11 days, on 24 February, an almost 5 ppt increase in the surface salinity occurred due to the 10 m/s northeasterly wind.

In terms of the NE storms, the upper layer drifts out of the bay due to downwind accelerations of the surface waters and the Coriolis force. This creates a shoreward undercurrent, leading the lower layer waters of the western basin to overflow the sill near the Hersek Delta. This novel finding indicates that the sill near the Hersek Delta acts as a control point for circulation. It is shown that only overflows are able to remove anoxia at the bottom of the central basin, as observed by Balkis [27].

Unlike the studies of [15,16], the western side of the model domain was defined as a lateral open boundary where the Orlanski radiation condition was prescribed. However, the Orlanski–BC in the west was insufficient to capture the influxes from the Black Sea and Mediterranean Sea via the water exchange between the bay and the Marmara Sea. Therefore, diffusion between layers became dominant, which decreased gradients in the thermocline and halocline. In NE 10.1 m/s and SE 10.1 m/s simulations, we predicted strong vertical mixing instead of overturning circulation due to the topographic shape of the bay and the reflection of the outgoing surface waters at the west, defined as Orlanski–BC. This reflection could be considered the adverse effect of the Istanbul Strait jet, which isolates the bay from the general circulation of the Marmara Sea [7]. In future modeling studies, a better definition of the water exchange between İzmit Bay and the Marmara Sea needs to be taken into account in order to improve the simulation of circulation.

The findings in this study are consistent with the characteristics of a bay's circulation response to wind, as described by Drinkwater [35]. The water circulation of İzmit Bay is also highly sensitive to the wind speed, direction, and duration; the size and shape of the bay, vertical stratification; and the oceanographic conditions in the adjacent offshore region. Severe wind can dominate the water exchange between the basins and the mixing between the layers. It also determines the physical features of the layers up to 60 m in depth. The water exchange between the basins, however, is limited by narrow passages, especially by the Hersek Delta, which controls both layers. Therefore, the role of the wind and topography should always be taken into consideration in pollution-monitoring studies (e.g., oil spill models, pollution distribution maps, etc.), coastal engineering projects (e.g., determination of wastewater discharge depth, port constructions, etc.), and scientific research (e.g., water quality, nutrient cycling, sedimentation, etc.) conducted in the bay.

**Author Contributions:** Conceptualization, S.M., B.Ö., M.I. and H.A.; methodology, S.M., B.Ö., M.I. and S.M. and H.A.; numerical modelling, S.M., M.I. and B.Ö.; validation, S.M. and B.Ö.; data curation, S.M. and B.Ö.; writing—original draft preparation, S.M.; writing—review and editing, B.Ö., M.I. and H.A.; visualization, S.M. and B.Ö.; supervision, B.Ö. All authors have read and agreed to the published version of the manuscript.

**Funding:** The authors thank the “Integrated Marine Pollution Monitoring 2017–2022 Program” funded by the Turkish Ministry of Environment and Urbanization/General Directorate of EIA, Permit and the SMART4ENV project (the European Union’s Horizon Europe research and innovation programme under Grant Agreement No. 101079251).

**Institutional Review Board Statement:** Not applicable.

**Informed Consent Statement:** Not applicable.

**Data Availability Statement:** The data presented in this study are available on request from the corresponding author.

**Acknowledgments:** We also thank all the crew of R/V TÜBİTAK MARMARA and the Marine Research & Technologies Group at The Vice Presidency of Climate Change and Sustainability of TÜBİTAK Marmara Research Centre for the provisioning of the data used in this study.

**Conflicts of Interest:** The authors declare no conflicts of interest.

### Appendix A

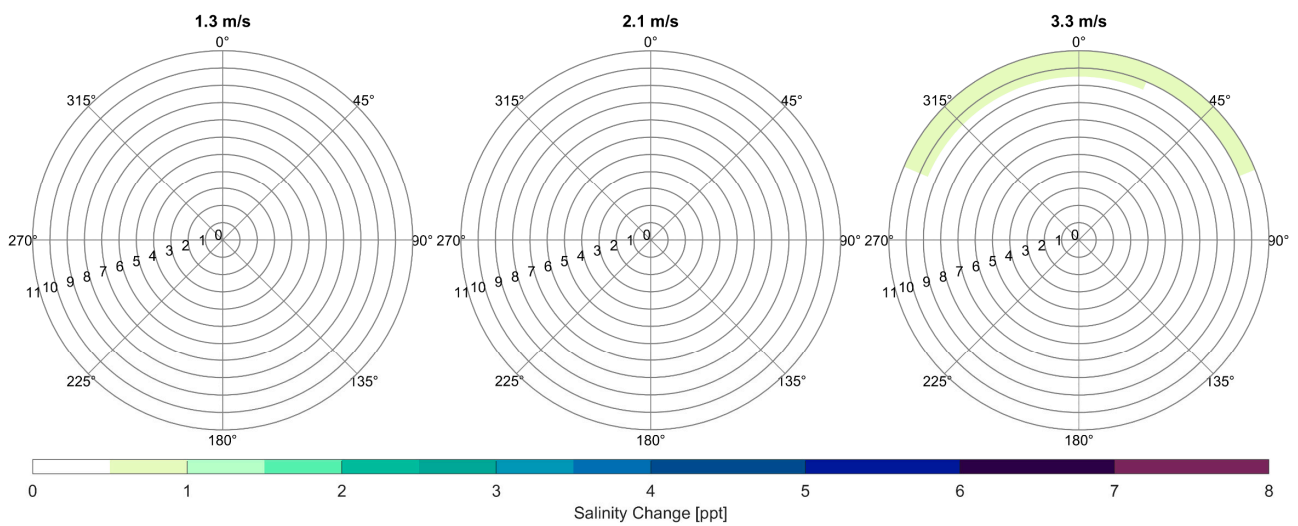


**Figure A1.** Surface salinity changes of the central basin based on wind direction sectors for corresponding weak wind speed simulations. Inner circles represent simulation days.

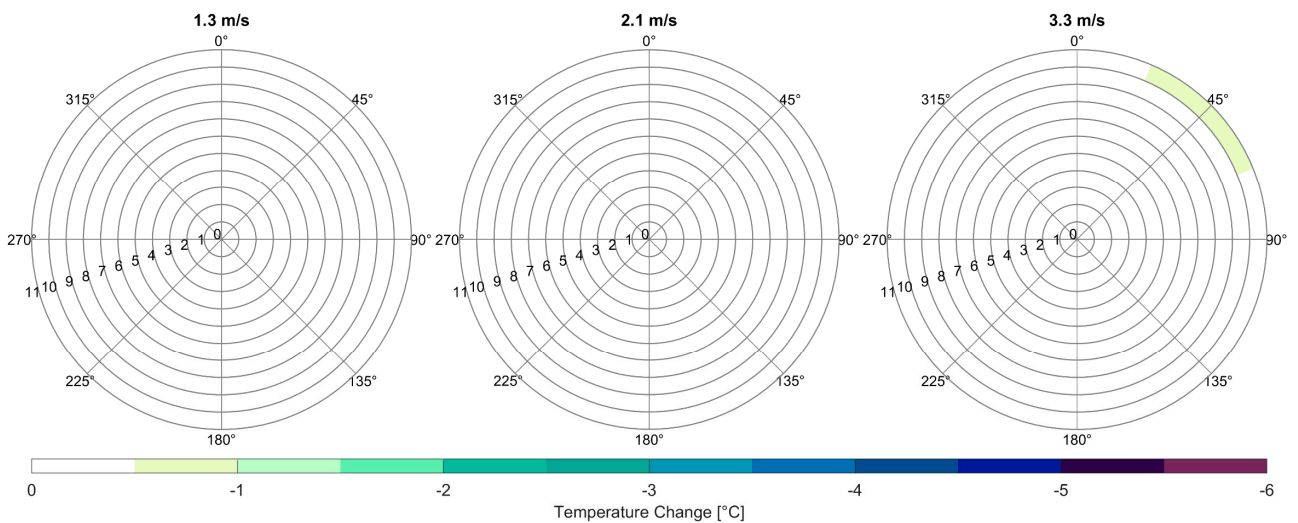


**Figure A2.** Surface temperature changes of the central basin based on wind direction sectors for corresponding weak wind speed simulations. Inner circles represent simulation days.

## References

- Ünlüata, Ü.; Oğuz, T.; Latif, M.A.; Özsoy, E. On the Physical Oceanography of the Turkish Straits. In *The Physical Oceanography of Sea Straits*; Pratt, L.J., Ed.; Springer: Dordrecht, The Netherlands, 1990; pp. 25–60. [CrossRef]
- Beşiktepe, Ş.T.; Sur, H.I.; Özsoy, E.; Latif, M.A.; Oğuz, T.; Ünlüata, Ü. The Circulation and Hydrography of the Marmara Sea. *Prog. Oceanogr.* **1994**, *34*, 285–334. [CrossRef]
- Tugrul, S.; Besiktepe, T.; Salihoglu, I. Nutrient Exchange Fluxes between the Aegean and Black Seas through the Marmara Sea. *Mediterr. Mar. Sci.* **2002**, *3*, 33–42. [CrossRef]
- Beşiktepe, Ş.T. Density Currents in the Two-Layer Flow: An Example of Dardanelles Outflow. *Oceanol. Acta* **2003**, *26*, 243–253. [CrossRef]
- Müftüoğlu, A.E. Marmara Denizi Halic ve Körfezlerinin Hidrodinamik Yapısı. Ph.D. Thesis, İstanbul University, İstanbul, Türkiye, 2008.
- Özsoy, E.; Altıok, H. A Review of Hydrography of the Turkish Straits System. In *The Sea of Marmara—Marine Biodiversity, Fisheries, Conservation and Governance*; Turkish Marine Research Foundation (TÜDAV): İstanbul, Türkiye, 2016; pp. 13–42.
- Özsoy, E. The Bosphorus Jet. In *The Sea of Marmara Marine Biodiversity, Fisheries, Conservation And Governance*; Turkish Marine Research Foundation (TÜDAV): İstanbul, Türkiye, 2016; pp. 135–149.
- Chiggiato, J.; Jarosz, E.; Book, J.W.; Dykes, J.; Torrisi, L.; Poulain, P.-M.; Gerin, R.; Horstmann, J.; Beşiktepe, Ş. Dynamics of the Circulation in the Sea of Marmara: Numerical Modeling Experiments and Observations from the Turkish Straits System Experiment. *Ocean Dyn.* **2012**, *62*, 139–159. [CrossRef]
- Sannino, G.; Sözer, A.; Özsoy, E. A High-Resolution Modelling Study of the Turkish Straits System. *Ocean Dyn.* **2017**, *67*, 397–432. [CrossRef]
- Aydoğdu, A.; Pinardi, N.; Özsoy, E.; Danabasoglu, G.; Gürses, Ö.; Karspeck, A. Circulation of the Turkish Straits System under Interannual Atmospheric Forcing. *Ocean Sci.* **2018**, *14*, 999–1019. [CrossRef]
- Ilicak, M.; Federico, I.; Barletta, I.; Mutlu, S.; Karan, H.; Ciliberti, S.A.; Clementi, E.; Coppini, G.; Pinardi, N. Modeling of the Turkish Strait System Using a High Resolution Unstructured Grid Ocean Circulation Model. *J. Mar. Sci. Eng.* **2021**, *9*, 769. [CrossRef]
- Baştürk, Ö.; Tuğrul, S.; Sunay, M.; Balkaş, T.; Morkoç, E.; Okay, O.S.; Bozyap, A. *Determination of Oceanographic Characteristics and Assimilation Capacity of İzmit Bay. NATO TU-WATERS Project*; Technical Report; TÜBİTAK-MRC Publication: Kocaeli, Turkey, 1985.
- Algan, O.; Altıok, H.; Yüce, H. Seasonal Variation of Suspended Particulate Matter in Two-Layered İzmit Bay, Turkey. *Estuar. Coast. Shelf Sci.* **1999**, *49*, 235–250. [CrossRef]
- Altıok, H.; Can, L.; Mutlu, S. Daily Variations in Stratification in İzmit Bay. *Turk. J. Earth Sci.* **2020**, *29*, 815–829. [CrossRef]
- Oğuz, T.; Sur, H.I. A Numerical Modelling Study of Circulation in the Bay of İzmit: Final Report. *TÜBİTAK MRC Chem. Dep. Publ. Kocaeli Turk.* **1986**, *187*, 97.
- Çehreli, Z.; Borekçi, O.S. İzmit Körfezi Akıntı Modellemesi. In *III. Ulusal Kıyı Mühendisliği Sempozyumu*; TMMOB İnşaat Mühendisleri Odası: Kızılay, Turkey, 2000.
- Morkoc, E.; Tarzan, L.; Okay, O.; Tufekci, H.; Tufekci, V.; Tolun, L.; Karakoc, F. Changes of Oceanographic Characteristics and the State of Pollution in the İzmit Bay Following the Earthquake of 1999. *Environ. Geol.* **2007**, *53*, 103–112. [CrossRef]
- Ergül, H.A. Evaluation of Seasonal Physicochemical Conditions and Chlorophyll-a Concentrations in İzmit Bay, Marmara Sea. *J. Black Sea/Mediterr. Environ.* **2016**, *22*, 201–217.
- Sur, H.İ. Numerical Modelling Studies of Two-Layer Flows in the Dardanelles Strait and the Bay of İzmit. Ph.D. Thesis, Middle East Technical University, Mersin, Türkiye, 1988.
- Yüce, H.; Alpar, B. Subtidal Sea-Level Variations in the Sea of Marmara, Their Interactions with Neighboring Seas and Relations to Wind Forcing. *J. Coast. Res.* **1997**, *13*, 1086–1092.
- GEBCO Bathymetric Compilation Group 2020. The GEBCO\_2020 Grid—A Continuous Terrain Model of the Global Oceans and Land. 2020. Available online: [https://www.bodc.ac.uk/data/published\\_data\\_library/catalogue/10.5285/a29c5465-b138-234-d-e053-6c86abc040b9/](https://www.bodc.ac.uk/data/published_data_library/catalogue/10.5285/a29c5465-b138-234-d-e053-6c86abc040b9/) (accessed on 1 December 2020).
- Taymaz, K.; Yigit, V.; Özbal, H.; Ceritoglu, A.; Müftügil, N. Heavy Metal Concentrations in Water, Sediment and Fish from İzmit Bay, Turkey. *Int. J. Environ. Anal. Chem.* **1984**, *16*, 253–265. [CrossRef]
- Tuğrul, S.; Sunay, M.; Baştürk, Ö.; Balkaş, T.I. The İzmit Bay Case Study. In *The Role of the Oceans as a Waste Disposal Option*; Kullenberg, G., Ed.; Springer: Dordrecht, The Netherlands, 1986; pp. 243–274. [CrossRef]
- Okay, O.S.; Tolun, L.; Telli-Karakoç, F.; Tüfekçi, V.; Tüfekçi, H.; Morkoç, E. İzmit Bay (Turkey) Ecosystem after Marmara Earthquake and Subsequent Refinery Fire: The Long-Term Data. *Mar. Pollut. Bull.* **2001**, *42*, 361–369. [CrossRef] [PubMed]
- Telli-Karakoç, F.; Tolun, L.; Henkelmann, B.; Klimm, C.; Okay, O.; Schramm, K.-W. Polycyclic Aromatic Hydrocarbons (PAHs) and Polychlorinated Biphenyls (PCBs) Distributions in the Bay of Marmara Sea: İzmit Bay. *Environ. Pollut.* **2002**, *119*, 383–397. [CrossRef] [PubMed]
- Ünlü, S.; Alpar, B. Hydrocarbon Balance of Surface Sediments in İzmit Bay (Marmara Sea), Turkey. *Bull. Env. Contam. Toxicol.* **2004**, *73*, 85–92. [CrossRef] [PubMed]
- Balkıs, N. The Effect of Marmara (İzmit) Earthquake on the Chemical Oceanography of İzmit Bay, Turkey. *Mar. Pollut. Bull.* **2003**, *46*, 865–878. [CrossRef] [PubMed]

28. Tüfekçi, V.; Balkis, N.; Beken, C.P.; Ediger, D.; Mantikci, M. Phytoplankton Composition and Environmental Conditions of the Mucilage Event in the Sea of Marmara. *Turk. J. Biol.* **2010**, *34*, 199–210. [CrossRef]
29. Tolun, L.G.; Ergenekon, S.; Hocaoglu, S.M.; Donertas, A.S.; Cokacar, T.; Husrevoglu, S.; Beken, C.P.; Baban, A. Socioeconomic Response to Water Quality: A First Experience in Science and Policy Integration for the Izmit Bay Coastal System. *Ecol. Soc.* **2012**, *17*, 40.
30. Ergül, H.A.; Aksan, S.; İpşiroğlu, M. Assessment of the Consecutive Harmful Dinoflagellate Blooms during 2015 in the Izmit Bay (the Marmara Sea). *Acta Oceanol. Sin.* **2018**, *37*, 91–101. [CrossRef]
31. Ülker, D.; Burak, S.; Balas, L.; Çağlar, N. Mathematical Modelling of Oil Spill Weathering Processes for Contingency Planning in Izmit Bay. *Reg. Stud. Mar. Sci.* **2022**, *50*, 102155. [CrossRef]
32. Kavzoglu, T.; Goral, M. Google Earth Engine for Monitoring Marine Mucilage: Izmit Bay in Spring 2021. *Hydrology* **2022**, *9*, 135. [CrossRef]
33. Wang, D.-P. Wind-Driven Circulation in the Chesapeake Bay, Winter, 1975. *J. Phys. Oceanogr.* **1979**, *9*, 564–572. [CrossRef]
34. Wind-Forced Motions in Stratified Lakes and Their Effect on Mixed-Layer Shear-Monismith-1985-Limnology and Oceanography-Wiley Online Library. Available online: <https://aslopubs.onlinelibrary.wiley.com/doi/10.4319/lo.1985.30.4.0771> (accessed on 23 April 2024).
35. Drinkwater, K.F. The Response of an Open Stratified Bay to Wind Forcing. *Atmosphere-Ocean* **1994**, *32*, 757–781. [CrossRef]
36. Llebot, C.; Rueda, F.J.; Solé, J.; Artigas, M.L.; Estrada, M. Hydrodynamic States in a Wind-Driven Microtidal Estuary (Alfacs Bay). *J. Sea Res.* **2014**, *85*, 263–276. [CrossRef]
37. Lips, U.; Laanemets, J.; Lips, I.; Liblik, T.; Suhhova, I.; Suursaar, Ü. Wind-Driven Residual Circulation and Related Oxygen and Nutrient Dynamics in the Gulf of Finland (Baltic Sea) in Winter. *Estuar. Coast. Shelf Sci.* **2017**, *195*, 4–15. [CrossRef]
38. Lai, W.; Pan, J.; Devlin, A.T. Impact of Tides and Winds on Estuarine Circulation in the Pearl River Estuary. *Cont. Shelf Res.* **2018**, *168*, 68–82. [CrossRef]
39. Mazoyer, C.; Vanneste, H.; Dufresne, C.; Ourmières, Y.; Magaldi, M.G.; Molcard, A. Impact of Wind-Driven Circulation on Contaminant Dispersion in a Semi-Enclosed Bay. *Estuar. Coast. Shelf Sci.* **2020**, *233*, 106529. [CrossRef]
40. Sheng, Y.P.; Liu, T. Three-Dimensional Simulation of Wave-Induced Circulation: Comparison of Three Radiation Stress Formulations. *J. Geophys. Res. Oceans* **2011**, *116*, C05021. [CrossRef]
41. Sun, Z.; Shao, W.; Wang, W.; Zhou, W.; Yu, W.; Shen, W. Analysis of Wave-Induced Stokes Transport Effects on Sea Surface Temperature Simulations in the Western Pacific Ocean. *J. Mar. Sci. Eng.* **2021**, *9*, 834. [CrossRef]
42. Delpey, M.T.; Ardhuin, F.; Otheguy, P.; Jouon, A. Effects of Waves on Coastal Water Dispersion in a Small Estuarine Bay. *J. Geophys. Res. Oceans* **2014**, *119*, 70–86. [CrossRef]
43. Lane, E.M.; Restrepo, J.M.; McWilliams, J.C. Wave-Current Interaction: A Comparison of Radiation-Stress and Vortex-Force Representations. *J. Phys. Oceanogr.* **2007**, *37*, 1122–1141. [CrossRef]
44. Gic-Grusza, G. The Three-Dimensional Wave-Induced Current Field: An Analytical Model. *Water* **2024**, *16*, 1165. [CrossRef]
45. Marshall, J.; Hill, C.; Perelman, L.; Adcroft, A. Hydrostatic, Quasi-hydrostatic, and Nonhydrostatic Ocean Modeling. *J. Geophys. Res. Oceans* **1997**, *102*, 5733–5752. [CrossRef]
46. Adcroft, A.; Hill, C.; Campin, J.-M.; Marshall, J.; Heimbach, P. Overview of the Formulation and Numerics of the MIT GCM. In Proceedings of the ECMWF Seminar Series on Numerical Methods, Recent Developments in Numerical Methods for Atmosphere and Ocean Modelling, Reading, UK, 6–10 September 2004; pp. 139–149.
47. Marshall, J.; Adcroft, A.; Hill, C.; Perelman, L.; Heisey, C. A Finite-volume, Incompressible Navier Stokes Model for Studies of the Ocean on Parallel Computers. *J. Geophys. Res. Oceans* **1997**, *102*, 5753–5766. [CrossRef]
48. Parkan, E.N. Comparison Between Hydrostatic And Nonhydrostatic Simulations Of Turkish Strait System. Master's Thesis, İstanbul Technical University, İstanbul, Türkiye, 2018.
49. Jackett, D.R.; McDougall, T.J. Minimal Adjustment of Hydrographic Profiles to Achieve Static Stability. *J. Atmos. Ocean. Technol.* **1995**, *12*, 381–389. [CrossRef]
50. Kämpf, J. Wind-Driven Overturning, Mixing and Upwelling in Shallow Water: A Nonhydrostatic Modeling Study. *J. Mar. Sci. Eng.* **2017**, *5*, 47. [CrossRef]
51. Greene, C.A.; Thirumalai, K.; Kearney, K.A.; Delgado, J.M.; Schwanghart, W.; Wolfenbarger, N.S.; Thyng, K.M.; Gwyther, D.E.; Gardner, A.S.; Blankenship, D.D. The Climate Data Toolbox for MATLAB. *Geochem. Geophys. Geosystems* **2019**, *20*, 3774–3781. [CrossRef]
52. Kämpf, J.; Möller, L.; Baring, R.; Shute, A.; Cheesman, C. The Island Mass Effect: A Study of Wind-Driven Nutrient Upwelling around Reef Islands. *J. Oceanogr.* **2023**, *79*, 161–174. [CrossRef]
53. Tilburg, C.E. Across-Shelf Transport on a Continental Shelf: Do across-Shelf Winds Matter? *J. Phys. Oceanogr.* **2003**, *33*, 2675–2688. [CrossRef]
54. Crise, A.; Querin, S.; Malačić, V. A Strong Bora Event in the Gulf of Trieste: A Numerical Study of Wind Driven Circulation in Stratified Conditions with a Preoperational Model. *Acta Adriat.* **2006**, *47*, 185–206.
55. Large, W.G.; McWilliams, J.C.; Doney, S.C. Oceanic Vertical Mixing: A Review and a Model with a Nonlocal Boundary Layer Parameterization. *Rev. Geophys.* **1994**, *32*, 363–403. [CrossRef]
56. Orlandi, I. A Simple Boundary Condition for Unbounded Hyperbolic Flows. *J. Comput. Phys.* **1976**, *21*, 251–269. [CrossRef]

- 
57. Querin, S.; Crise, A.; Deponte, D.; Solidoro, C. Numerical Study of the Role of Wind Forcing and Freshwater Buoyancy Input on the Circulation in a Shallow Embayment (Gulf of Trieste, Northern Adriatic Sea). *J. Geophys. Res. Oceans* **2006**, *111*, 2006JC003611. [[CrossRef](#)]
  58. Öztürk, M.; Yüksel, Y. Tidal and Non-Tidal Sea Level Analysis in Enclosed and Inland Basins: The Black, Aegean, Marmara, and Eastern Mediterranean (Levantine) Seas. *Reg. Stud. Mar. Sci.* **2023**, *61*, 102848.

**Disclaimer/Publisher's Note:** The statements, opinions and data contained in all publications are solely those of the individual author(s) and contributor(s) and not of MDPI and/or the editor(s). MDPI and/or the editor(s) disclaim responsibility for any injury to people or property resulting from any ideas, methods, instructions or products referred to in the content.